Biophysical *Journal*
Article

Biophysical Society

A Role for Weak Electrostatic Interactions in Peripheral Membrane Protein Binding

Hanif M. Khan,[1,2] Tao He,[3] Edvin Fuglebakk,[1,2] Cédric Grauffel,[1,2] Boqian Yang,[3,4] Mary F. Roberts,[3] Anne Gershenson,[4] and Nathalie Reuter[1,2,*]

[1]Department of Molecular Biology and [2]Computational Biology Unit, Department of Informatics, University of Bergen, Bergen, Norway; [3]Department of Chemistry, Boston College, Chestnut Hill, Massachusetts; and [4]Department of Biochemistry and Molecular Biology, University of Massachusetts, Amherst, Massachusetts

ABSTRACT *Bacillus thuringiensis* phosphatidylinositol-specific phospholipase C (*Bt*PI-PLC) is a secreted virulence factor that binds specifically to phosphatidylcholine (PC) bilayers containing negatively charged phospholipids. *Bt*PI-PLC carries a negative net charge and its interfacial binding site has no obvious cluster of basic residues. Continuum electrostatic calculations show that, as expected, nonspecific electrostatic interactions between *Bt*PI-PLC and membranes vary as a function of the fraction of anionic lipids present in the bilayers. Yet they are strikingly weak, with a calculated ΔG_{el} below 1 kcal/mol, largely due to a single lysine (K44). When K44 is mutated to alanine, the equilibrium dissociation constant for small unilamellar vesicles increases more than 50 times (~2.4 kcal/mol), suggesting that interactions between K44 and lipids are not merely electrostatic. Comparisons of molecular-dynamics simulations performed using different lipid compositions reveal that the bilayer composition does not affect either hydrogen bonds or hydrophobic contacts between the protein interfacial binding site and bilayers. However, the occupancies of cation-π interactions between PC choline headgroups and protein tyrosines vary as a function of PC content. The overall contribution of basic residues to binding affinity is also context dependent and cannot be approximated by a rule-of-thumb value because these residues can contribute to both nonspecific electrostatic and short-range protein-lipid interactions. Additionally, statistics on the distribution of basic amino acids in a data set of membrane-binding domains reveal that weak electrostatics, as observed for *Bt*PI-PLC, might be a less unusual mechanism for peripheral membrane binding than is generally thought.

INTRODUCTION

The association of peripheral membrane proteins with biological membranes is classically described as an electrostatically driven approach followed by the intercalation of hydrophobic groups into the lipid bilayer. Long-range, nonspecific electrostatic forces between the negatively charged membrane and clusters of basic amino acids bring the protein into a binding-competent orientation relative to the lipid bilayer and play a major role for numerous prototypical peripheral membrane proteins (1–4). Experimental and pioneering computational studies have revealed that nonspecific electrostatic interactions contribute a few kilocalories per mole to the overall affinity. It is also estimated that each basic amino acid contributes up to 1 kcal/mol to the binding free energy (2,5).

Bacillus thuringiensis phosphatidylinositol-specific phospholipase C (*Bt*PI-PLC) is a 34.8 kDa secreted virulence factor that carries a negative net charge (−7 e) and binds most tightly to phosphatidylcholine (PC) bilayers containing negatively charged phospholipids, (e.g., phosphatidylglycerol (PG), phosphatidylserine, phosphatidic acid, and phosphatidylinositol (6)). Its interfacial binding site (IBS) consists of a small α-helix, helix B (7), and two neighboring loops rich in tyrosines that we have shown engage in cation-π interactions with the choline groups of dimyristoylphosphatidylcholine (DMPC) lipids in neutral bilayers (8). These cation-π interactions provide a likely molecular mechanism for *Bt*PI-PLC's PC specificity (8,9), but do not account for its preference for bilayers containing a small fraction of anionic lipids (10).

The affinity of *Bt*PI-PLC has been measured to be tightest for vesicles containing PC and 20% anionic lipids. For this composition, the affinity is ~4 times more favorable than that for neutral vesicles, and a higher anionic lipid content decreases the affinity considerably (10). Surprisingly, under the tightest binding conditions, mutating a single lysine

Submitted August 26, 2015, and accepted for publication February 2, 2016.

*Correspondence: nathalie.reuter@uib.no

Cédric Grauffel's present address is Institute of Biomedical Sciences, Academia Sinica, Taipei, Taiwan.

Editor: Scott Feller.

http://dx.doi.org/10.1016/j.bpj.2016.02.020

(K44) to an alanine decreases the binding affinity to 1/55th of that of the wild-type (WT) protein, corresponding to ~2.4 kcal/mol. This effect is of the same order of magnitude as the mutation of hydrophobic amino acids of helix B and is ~14 times greater than the fourfold loss of binding affinity observed for binding to pure PC vesicles versus vesicles containing PC and 20% anionic lipids. If mutating K44 affects only the nonspecific electrostatic forces involved in the adsorption of protein onto the phospholipid bilayer, the effect of removing the anionic lipids should be comparable to that of mutating K44 and the other basic amino acids. Furthermore, the effect of the K44A mutation on the affinity of *Bt*PI-PLC toward negatively charged vesicles is strikingly high compared with values found in the literature (2,5).

Here, we investigate the forces that drive *Bt*PI-PLC's specificity for negatively charged PC-containing vesicles by separately addressing the two steps that govern membrane affinity: association (k_{on}) and dissociation (k_{off}). Although the former is fast, the dissociation that follows is comparatively slow and constitutes the rate-limiting step. As a consequence, in systems where the protein binds to the membrane without undergoing significant conformational changes or interacting with another protein, the affinity for the membrane is mostly accounted for by interactions between the protein IBS and lipids. As these interactions are difficult to assess experimentally, molecular dynamics (MD) simulations are widely used to evaluate IBS-lipid interactions (11–14).

Using multiple 500-ns-long MD simulations of *Bt*PI-PLC at the surface of pure DMPC, pure dimyristoylphosphatidylglycerol (DMPG), and mixed DMPC/DMPG (composition described by mole fraction PC, X_{PC}) bilayers, we mapped specific protein-lipid interactions and investigated how these interactions are influenced by the anionic lipid content. We also evaluated the nonspecific electrostatic contributions of key basic amino acids to the association step using continuum electrostatic calculations, which were previously used to quantify the role of electrostatics in protein-membrane association (15,16). We determined experimentally the effect of mutating key basic amino acids to alanine by using fluorescence correlation spectroscopy (FCS) to measure the affinity of *Bt*PI-PLC variants for small unilamellar vesicles (SUVs). Combining the computational and experimental data allowed us to formulate a complete model of *Bt*PI-PLC membrane binding. A novel characteristic of this model is the unusually weak nonspecific electrostatic contribution due to the curiously low number and distribution of lysines and arginines on the *Bt*PI-PLC surface. The rather unexpected character of this finding led us to evaluate how (un)common such a distribution is among peripheral membrane proteins. We thus analyzed the number and distribution of basic amino acids in a database of peripheral membrane-binding proteins, and found that a significant number of peripheral membrane proteins are highly likely to also display weak nonspecific electrostatics. We propose that such weak interactions could be beneficial for the function of some classes of peripheral membrane proteins, particularly those that must exhibit a quick response to environmental changes.

MATERIALS AND METHODS

MD simulations

As no x-ray structure is available for WT *Bt*PI-PLC, we built a model as described by Grauffel et al. (8), using the x-ray crystal structures of the *Bt*PI-PLC Y247S/Y251S (17) (PDB ID: 3EA1) and W47A/W242A (18) (PDB ID: 2OR2) mutants. The starting orientation of bilayer-bound *Bt*PI-PLC was obtained from the same study and based on implicit membrane simulations (8).

The protocol used for bilayer preparation is described in Supporting Materials and Methods in the Supporting Material. The protein was manually docked on the preequilibrated mixed bilayers as described in Grauffel et al. (8), using membrane orientations obtained from *Bt*PI-PLC MD simulations with an implicit membrane model (8). Lipids located within 2 Å of the protein were removed to avoid coordinate overlap and steric clashes. The system was then minimized as described by Grauffel et al. (8) and solvated with TIP3P water molecules using VMD (19). After solvation, if the system had a net charge, additional sodium ions were added by randomly replacing water molecules to achieve an overall charge neutral system.

MD simulations of bilayer-bound BtPI-PLC

The combined protein-lipid system was then subjected to two short (400 ps) equilibrations in the NVT ensemble with constraints on the protein backbone. Subsequently, we equilibrated the system for 2 ns in the NPT ensemble without any constraints before finally performing the 500 ns NPT simulation. The temperature was set to 310 K during the simulation with a 2 fs integration time step in NAMD (v2.9) (20). In all cases the temperature was controlled using Langevin dynamics (temperature damping coefficient: 1.0) and the pressure was set to 1 atm using the Langevin piston method (21) with an oscillation period of 200 fs and a damping timescale of 50 fs. The CHARMM all-atom force field (22) (c22 including the CMAP correction) (23) and the force field update for lipids (CHARMM36) (24) were then used for all of the 500 ns simulations. Trajectory conformations were saved every 10 ps. Two simulations were performed for each lipid composition, and in the second replicate the protein was rotated by 180° around the bilayer normal (z axis) to allow for different initial protein-lipid contacts. This rotation was done to avoid bias in protein-lipid interactions due to the initial distribution of lipids under or around the protein, and also to improve the sampling. Analyses of the trajectories were performed using CHARMM (v33b1) (25) and VMD (v1.9.1) (19) on the last 450 ns of each simulation in a manner similar to that described in Grauffel et al. (8).

We first checked that the simulations had converged. All simulations with $X_{PC} > 0$ converged to a stable *Bt*PI-PLC anchorage at similar insertion depths and with no significant structural changes compared with the x-ray crystal structure. The backbone root mean-square deviation (RMSD) is at most 1.61 Å (see Supporting Materials and Methods; Table S2). Moreover, the interactions between protein amino acids and lipids converge to a pattern that is reproduced by both replicas. Hydrophobic interactions and hydrogen bonds were assigned as described in Supporting Materials and Methods. Cation-π interactions between the aromatic amino acids (Tyr, Phe, and Trp) and the choline group of the DMPC lipids were assigned as described earlier (8,26). Hydrophobic contacts, hydrogen bonds, and cation-π interactions were averaged over the two replicas.

Continuum electrostatic calculations

We extracted the structures of the bilayers after the simulations to perform continuum electrostatic calculations by solving the Poisson-Boltzmann

(PB) equation. These equilibrated bilayers provide a better description of the membrane than ideal flat bilayers (i.e., nonequilibrated lipid bilayers) such as those used in previous studies (15,16). For these calculations, we prepared the protein-membrane complex by placing the protein with its membrane-binding orientation above the bilayer upper leaflet. We defined the minimum protein-membrane distance (d) as the z distance between the HD1 atom of Ile43 and the maximum z coordinate of the bilayer. HD1 is a hydrogen atom on the Cδ atom of Ile43 and was chosen because it is the most deeply anchored atom in the membrane-binding conformation. The initial position of the protein was set to $d = 12$ Å. The protein was then gradually translated toward the membrane. Both the protein and the membrane were kept rigid. PB calculations of the electrostatic potential were carried out using APBS (version 1.3) (27). This electrostatic potential and those obtained from the bilayer and the protein were then used to calculate the electrostatic free energy (28,29). A similar scheme has been used for other proteins (15,16,30). The nonpolar contribution to the binding free energy was not evaluated, as that was not the goal of this work.

Database statistics

The statistics for net charges and the distributions of basic amino acids in peripheral membrane proteins were obtained from a curated data set based on the Orientations of Proteins in Membranes (OPM) database (31). This database contains membrane-associated proteins and predictions of their orientation in a DOPC bilayer model. We selected all protein families of the OPM classification type monotopic/peripheral, for a total of 337 families. For each selected family, we obtained the average net charges, $\widehat{c}_F$. We defined solvent-exposed residues to be those with at least 20% of their surface contributing to the protein surface in its maximal exposure. Using MMTK (32), we calculated the surface contributions from each atom using a radius around the atom equal to the sum of its van der Waals radius and a fixed 1.4 Å term to mimic water accessibility. Maximal exposure for each residue type was obtained from a random-coil model (33). We defined the insertion coordinate, i, of a point to be the distance from that point to the end of the hydrocarbon region of the membrane in the membrane model employed in the OPM database (34). This distance was made negative for points on either of the hydrated sides of the membrane of the membrane. We use $n_p^{\text{basic}}(z,x)$ to denote the number of solvent-exposed basic amino acids in protein, p, that have α carbons with insertion coordinates $z \le i$ and $i < x$. The number of basic amino acids at the IBS is then taken to be n_p^{basic} (0, −10 Å), and we report the family average, w_F^{basic}. We also calculated the average surface density of basic amino acids at varying distances from the membrane $(n_p^{\text{basic}}(z,x)/n_p^{\text{any}}(z,x))$, which we report as d_S^{basic} (more details are provided in Supporting Materials and Methods).

Expression and purification of *Bt*PI-PLC and its variants

All *Bt*PI-PLC mutants were constructed from the plasmid containing the mutant N168C *Bt*PI-PLC gene, using a QuikChange Site-Directed Mutagenesis Kit from Agilent Technologies (Santa Clara, CA). The Cys at 168 was used to fluorescently label the proteins for FCS experiments. Mutated genes were sequenced to ensure that the correct mutations had been incorporated and no other mutations had arisen. All *Bt*PI-PLC variants expressed at high levels in *Escherichia coli* and were purified in two chromatographic steps (elution on a Q-Sepharose fast-flow column and then on a phenyl-Sepharose column) as described previously for recombinant *Bt*PI-PLC (35). More than 90% purity was achieved as monitored by SDS-PAGE. Protein solutions were concentrated and the protein concentration was calculated from the absorption at 280 nm using extinction coefficients estimated by ProtParam (36). The composition of secondary-structure elements, estimated from far-UV circular dichroism data, was essentially the same for all of the variants, indicating that no significant secondary-structure changes had occurred (see Table S9). We assessed the thermal stability of *Bt*PI-PLC by using far-UV circular dichroism and monitoring the ellipticity at 222 nm while increasing the sample temperature 0.5° per minute (7,37). We determined the specific activities of all variants (see Supporting Materials and Methods) toward SUVs prepared by sonication and composed of 2 mM phosphatidylinositol (PI) plus various concentrations of 1-palmitoyl-2-oleoyl-phosphatidylcholine (POPC) in 50 mM HEPES (containing 1 mg/mL bovine serum albumin), pH 7.5. For pure PI and PI/PC (4:1) SUVs, the total phospholipid concentration was below or comparable to the K_d; hence, the mutant-specific activities were lower than observed for the WT enzyme. For PI/PC SUVs with $X_{PC} = 0.5$ and 0.8, the total phospholipid concentration was above the apparent K_d for all of the Lys/Arg to Ala mutants except K44A. Specific activities were measured by ^{31}P NMR spectroscopy as described previously (6,10). All phospholipids were obtained from Avanti Polar Lipids (Alabaster, AL).

FCS measurements of *Bt*PI-PLC binding to SUVs

FCS-based SUV binding experiments take advantage of the fact that protein binding to vesicles slows translational diffusion. FCS experiments were performed using *Bt*PI-PLC variants labeled at N168C with Alexa Fluor 488 maleimide and an in-house-built confocal setup based on an IX-70 inverted microscope (Olympus, Center Valley, PA) as previously described (37) (see Supporting Materials and Methods). SUVs composed of PG and PC were prepared by sonication of rehydrated lipid films. The compositions are denoted by X_{PC}, the mole fraction of PC.

RESULTS

Influence of PC content on short-range specific protein-lipid interactions

To determine the roles of short-range protein-lipid interactions in *Bt*PI-PLC membrane affinity, and to identify the interactions responsible for lipid specificity, we performed multiple 500-ns-long MD simulations for *Bt*PI-PLC docked to preequilibrated DMPC/DMPG bilayers with four different DMPC mole fractions: $X_{PC} = 0$, 0.5, 0.8, and 1.0 (Supporting Materials and Methods; Table S1). The results for $X_{PC} = 1.0$ were taken from earlier reported simulations (8). Although the residence time of *Bt*PI-PLC on SUVs has been measured to be a few hundreds of milliseconds (9), the use of shorter MD simulations to map relevant protein-lipid interactions has proven reliable (8,9,38). To avoid bias due to the initial distribution of lipids around the protein, we repeated all of the simulations using different initial protein positions in the membrane plane. We also performed a simulation using the K44A *Bt*PI-PLC mutant bound to an anionic membrane ($X_{PC} = 0.8$).

Interactions with a pure DMPG bilayer ($X_{PC} = 0$)

Both simulations of WT *Bt*PI-PLC docked to pure DMPG bilayers indicated loose binding of the protein to pure DMPG bilayers compared with DMPC-containing bilayers. In one of the simulations, the protein completely detached from the bilayer within 200 ns (Fig. 1). In the other simulation, the protein remained bound but the structure of the β7-αG loop (also called the rim loop) became distorted (Fig. 2). The average backbone RMSD of β7-αG along the simulation time is 1.8 ± 0.4 Å, compared with

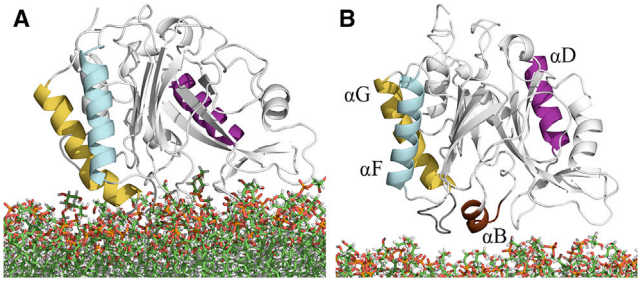

FIGURE 1 Snapshots from one of the MD simulations of WT *Bt*PI-PLC on a DMPG bilayer ($X_{PC} = 0$, replica 2). (*A*) System at the beginning of the production run. (*B*) System after 200 ns. *Bt*PI-PLC is represented by cartoons and the lipids are shown with sticks. The secondary-structure elements relevant for this study are labeled: helix B, αB; helix D, αD; helix F, αF; helix G, αG. For the sake of clarity, water molecules and ions are not shown. To see this figure in color, go online.

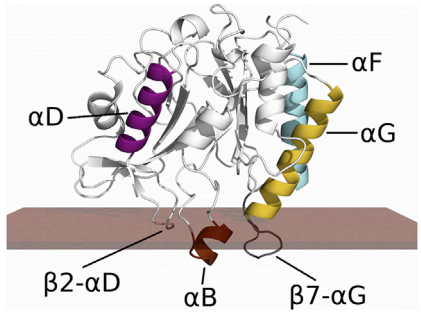

FIGURE 3 *Bt*PI-PLC secondary-structure elements and their calculated insertion at the interface of a mixed DMPC/DMPG bilayer ($X_{PC} = 0.5$). *Bt*PI-PLC is represented by cartoons. The relevant secondary-structure elements are labeled as in Fig. 1. Helix B is inserted beyond the phosphate plane (*dark slab*) of the mixed bilayer. To see this figure in color, go online.

0.4 ± 0.1 Å in simulations with PC-containing bilayers (see Fig. S1). Compared with those simulations, we also observed a loss of long-lived backbone hydrogen bonds (N243-G238, N243-T240, and Y248-S244) in the rim loop. A similar distortion of the β7-αG loop was observed in simulations of the free Y248A variant, which showed impaired lipid binding with an apparent K_d ~150 times higher than that of WT *Bt*PI-PLC toward vesicles with $X_{PC} = 1$ (8).

Interactions with DMPC/DMPG bilayers: X_{PC} = [0.5, 0.8, 1]

All of the simulations with bilayers containing PC lipids yielded stable *Bt*PI-PLC anchorage, with no significant structural changes compared with the x-ray crystal structure. The backbone RMSD is at most 1.61 Å (average values for each simulation are provided in Table S2). The protein anchored helix B and the rim loop in the bilayer interface (Fig. 3) at similar depths (Fig. 4) independently of the PC lipid content.

For each of the three bilayer compositions, we inventoried the interactions that occurred between the bilayer lipids and protein residues located at the interface. We report in Table 1 the numbers of hydrogen bonds, hydrophobic contacts, and cation-π interactions per frame, averaged over each of the bilayer compositions and replicas (the corresponding values per amino acid are provided in Table S3). Briefly, three main *Bt*PI-PLC regions mediate most of the interactions with lipids, namely, helix B, the β2-αD loop, and the β7-αG loop. Helix B anchors deepest, with most of its amino acids below the phosphate plane (Figs. 3 and 4). Residues 238–242 of the β7-αG loop are also inserted below the average phosphate plane (Table S4). All three anchored regions mediate hydrophobic interactions with multiple lipid tails; for example, helix B mediates 25–26 hydrophobic contacts irrespective of the PC content in the bilayer (Fig. 5 *A*). The hydrophobic contacts mediated by *Bt*PI-PLC with the lipids do not vary significantly with X_{PC}. The same applies to hydrogen bonds. We observe long-lived hydrogen bonds between lipid phosphate groups and the side chains of charged (K44, R71, K122, and K201), polar (S236 and S244), and aromatic residues (Y88, Y246, Y247, and Y251), as well as the backbones of polar residues (Q40 and N41). However, there is no correlation between the number and stability of these hydrogen bonds and the mole ratio of PC lipids in the bilayers.

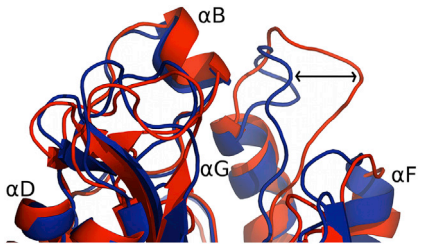

FIGURE 2 Comparison of the *Bt*PI-PLC membrane-bound secondary structure after a 500 ns simulation for $X_{PC} = 0$ (*red*, pure DMPG) and $X_{PC} = 0.5$ (*blue*). The backbone structures were aligned using PyMOL (39). For the sake of clarity, lipids, water molecules, and ions are not shown. The essential intramolecular interactions within the rim loop (β7-αG) are lost at $X_{PC} = 0$, causing a distorted loop structure (*arrow*). To see this figure in color, go online.

The trend is different for cation-π interactions between choline headgroups of PC lipids and tyrosines. The overall number of cation-π interactions clearly increases with PC enrichment. In a previous study (8), we reported that Y88, Y204, Y246, or Y251 engaged in high-occupancy cation-π interactions in simulations of *Bt*PI-PLC with pure DMPC bilayers. Here, upon addition of DMPG to the bilayers, we observed that the occupancy of cation-π interactions varied with X_{PC} (Fig. 5 *B*). The occupancies of the cation-π interactions mediated by Y246, Y251, and Y204 increased from $X_{PC} = 0.5$ to $X_{PC} = 0.8$, but not significantly between $X_{PC} = 0.8$ and 1.0. Although we ensured that the simulations were not biased by the initial lipid distribution, we cannot rule out the possibility that this apparent saturation is an artifact of the relatively short timescale of our simulations. Y88 and Y246 are located close to the IBS and mediate the cation-π interactions with the highest

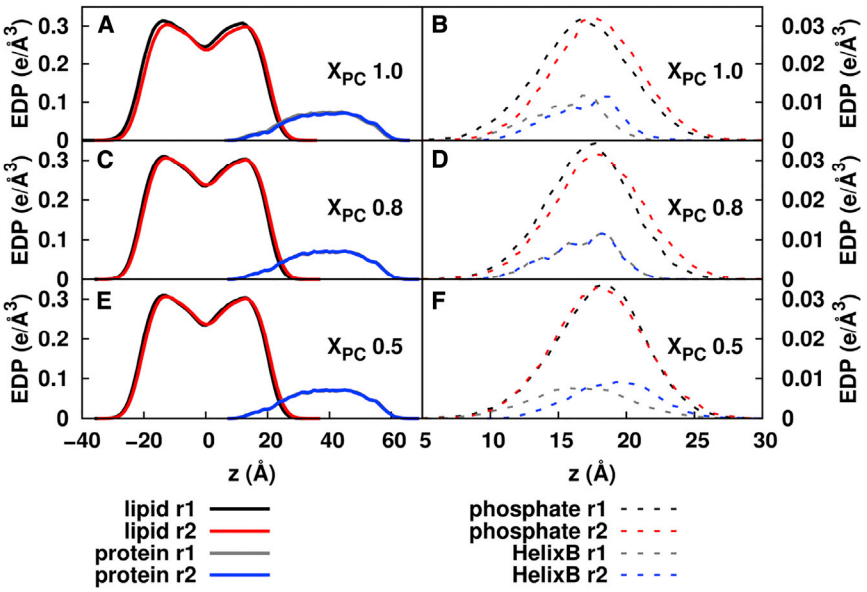

FIGURE 4 Electron density profiles (EDPs) from MD simulations for three different bilayers. (*A*, *C*, and *E*) Protein and lipids (r1, replica 1; r2, replica 2) for X_{PC} = 1, 0.8, and 0.5. (*B*, *D*, and *F*) Deepest inserted helix (αB) and phosphate groups of the upper lipid leaflet. Note that the plain lines for protein r1 and protein r2 overlap almost perfectly. To see this figure in color, go online.

occupancy. They are also the Tyr residues whose mutation to alanine has the largest effect on a protein's affinity for SUVs (8) (also see Fig. S2). Overall, the occupancy of these interactions for tyrosines 86, 88, 204, 246, 247, and 251 correlates qualitatively with the effects of their mutation to alanine on *Bt*PI-PLC's affinity for SUVs (cf. Grauffel et al. (8) and Fig. S2). Y251 is the only tyrosine that we observed to mediate two cation-π interactions simultaneously, with an occupancy of up to 11% at X_{PC} = 0.8 (r1), which may be due to the accessibility of its side chain to PC lipids (see Tables S5 and S6).

Interactions of BtPI-PLC K44A with a mixed bilayer: X_{PC} = 0.8

Experimental data indicate that mutating K44 to alanine drastically affects the affinity of *Bt*PI-PLC for SUVs. Here, we investigated the effect of this mutation on specific protein-lipid interactions by docking K44A *Bt*PI-PLC on a mixed bilayer (X_{PC} = 0.8). In contrast to simulations with a pure DMPG bilayer or the Y248A mutant in water (8), K44A remained bound to the membrane surface with an unaltered structure. The average RMSD of the protein backbone along the simulation time relative to the energy-minimized K44A structure is 1.5 ± 0.2 Å. An analysis of the depth of anchorage for different amino acids shows that there is negligible variation along the simulation, but major interactions are lost (cf. Table S7). In particular, an important protein-lipid hydrogen-bond network around helix B, involving Q40 and N41 backbone atoms, the K44 side chain, and DMPC phosphates, is lost (8). As a consequence, the number of hydrogen bonds mediated by helix B is low compared with the WT. Moreover, helix B mediates slightly fewer hydrophobic contacts per frame (24.7 vs. 25.7, respectively). As might be expected, the occupancies of the cation-π interactions are generally comparable to those observed for WT *Bt*PI-PLC.

TABLE 1 Inventory of Interactions with Pure DMPC and Mixed Bilayers

	X_{PC}		
Interactions	0.5	0.8	1.0
Hydrogen bonds	7.9/4.4	7.0/7.6	7.8/6.9
Hydrophobic contacts	49.2/41.1	41.7/40.2	45.0/42.3
Cation-π	2.5/2.2	2.8/2.9	3.6/3.0

The average numbers of hydrogen bonds, hydrophobic contacts, and cation-π per frame are given for each replica (r1/r2).

Nonspecific electrostatic interactions upon membrane association

The *Bt*PI-PLC IBS includes five lysines (K38, K44, K122, K201, and K279) and one arginine. Whereas K44 is located on helix B, the four other lysines and one arginine (R71) are carried by other structural elements and do not form the

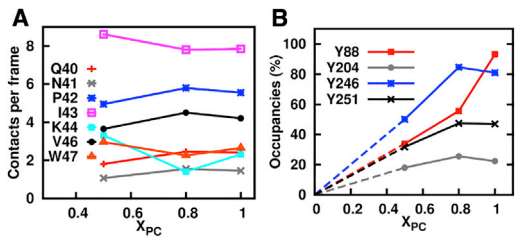

FIGURE 5 Influence of bilayer composition on short-range protein-lipid interactions. (*A*) Average number of hydrophobic contacts per frame between helix B amino acids and the bilayer lipids as a function of X_{PC}. The membrane composition has no significant effect on hydrophobic insertion. (*B*) Cation-π interactions between Tyr amino acids and choline headgroups of DMPC lipids. The occupancies along the simulation are plotted with respect to the membrane PC content. To see this figure in color, go online.

obvious cluster(s) that are often described for membrane-binding domains. This leads us to ask about the magnitude of *nonspecific* electrostatic interactions between proteins and negatively charged membranes.

Electrostatic free-energy profile

We calculated the electrostatic component of the binding free energy by using continuum electrostatics and solving the PB equation (cf. Supporting Materials and Methods and Fig. S3). This approach has been successfully used to describe the electrostatic properties of proteins, nucleic acids, and membranes (27,40,41). Note that the chosen approach only allows us to reasonably estimate the electrostatic contribution when the protein is above the modeled membrane and not at its most favorable anchorage depth. The latter is measured by the MD simulations presented above to be ~8–10 Å below the membrane surface, as measured by the position of the center of mass of isoleucine 43, the deepest-anchored residue.

Electrostatic potential isocontours at ± 1 k_BT/e for *Bt*PI-PLC (Fig. 6 *A*) show large negative regions. The positive regions are more restricted in size, with one of the larger positive regions located around helix B. The profile of the electrostatic free energy for WT approaching a negatively charged bilayer (DMPC/DMPG, $X_{PC} = 0.8$) shows a minimum at a protein-membrane distance, *d*, of 3–4 Å (Fig. 7). The electrostatic free energy is at most −0.25 kcal/mol, much lower than that reported for other membrane-binding domains using the same computational approach (from −3 to −5 kcal/mol) (16). The electrostatic free energy becomes less favorable as the protein moves toward the membrane from this minimum, eventually becoming unfavorable when the protein is in contact with the membrane surface (+0.4 kcal/mol) and crosses the upper limit of the membrane (+1.1 kcal/mol) (Fig. 7). The favorable contribution is largely due to K44, and the K44A mutation almost completely abolishes the favorable ΔG_{el} (Figs. 6 *B* and 7). Mutations at other positively charged residues (K38, R71, K122, K201, and K279) affect ΔG_{el} to a lesser extent, with a value of ~−0.1 kcal/mol at the most favorable distance.

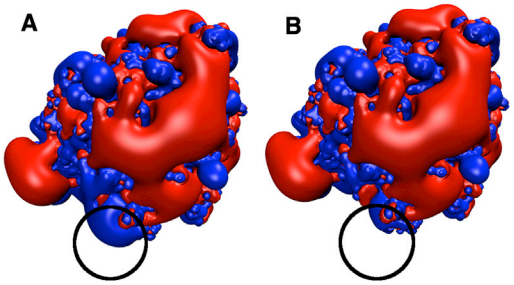

FIGURE 6 (*A* and *B*) Calculated electrostatic potentials of (*A*) WT *Bt*PI-PLC and (*B*) K44A. The isocontours at +1 kBT/e (*blue*) and −1 kBT/e (*red*) are shown. Note the change of the isosurface around the K44A mutation site in helix B (*black circle*). The images were prepared using VMD (19). To see this figure in color, go online.

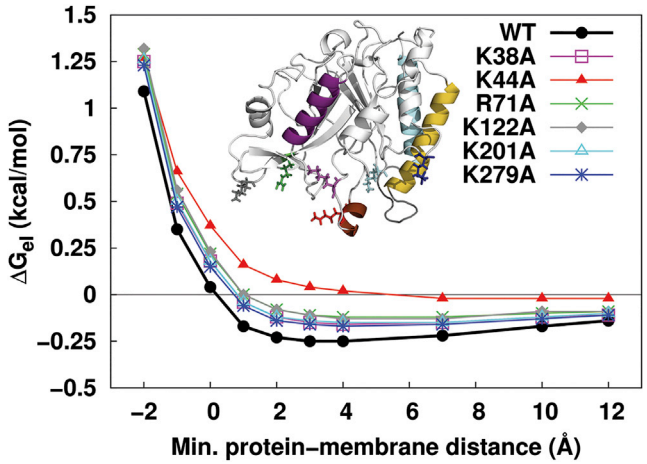

FIGURE 7 Electrostatic free-energy profile of WT and mutants with an anionic membrane ($X_{PC} = 0.8$), using a 0.1 M salt concentration. A hydrogen atom in Ile43 (CHARMM nomenclature HD1) is the closest *Bt*PI-PLC atom to the membrane in the membrane-binding orientation, where the approach is along the *z* axis perpendicular to the membrane. The position of this atom relative to the membrane is decreased to drag the protein toward the membrane while keeping both the protein and the membrane rigid. Errors arising from grid spacing are evaluated to be <0.003 kcal.mol^{-1} (for details, see Supporting Materials and Methods). To see this figure in color, go online.

Effect of membrane composition and salt concentration

We evaluated the dependence of the protein electrostatic free energy on lipid composition by calculating the electrostatic free energy at $d = 3$ Å for decreasing ratios of DMPC lipids ($X_{PC} = 1.0$, 0.8, 0.5, and 0) (Fig. 8 *A*). The electrostatic free energy is slightly unfavorable for a neutral membrane (0.1 kcal/mol) and decreases monotonically with the PC content until $X_{PC} = 0.5$ ($\Delta G_{el} = -0.68$ kcal/mol). It then increases to −0.42 kcal/mol with X_{PC} decreasing to zero, in agreement with experimental data (42).

We further calculated ΔG_{el} for $d = 3$ Å and $X_{PC} = 0.8$ at salt concentrations ranging from 0.025 to 0.7 M (Fig. 8 *B*). *Bt*PI-PLC shows a quasi-parabolic dependence of the electrostatic free energy on salt concentration. At the lowest ionic strength tested (0.025 M), the electrostatic free energy of interaction between the protein and the membrane is slightly unfavorable (0.08 kcal/mol). It then quickly becomes more favorable until a salt concentration of 0.1 M (−0.25 kcal/mol) is reached, which is also approximately the physiological ionic strength surrounding the target eukaryotic cell. It then gradually becomes less favorable with increasing salt concentrations. This behavior can be explained by the fact that the unfavorable interactions between the protein and the bilayer are not significantly screened at low salt concentrations (see the large negative electrostatic potential isocontours shown in Fig. 6 *A*). However, it is important to note that the electrostatic partitioning of *Bt*PI-PLC is low.

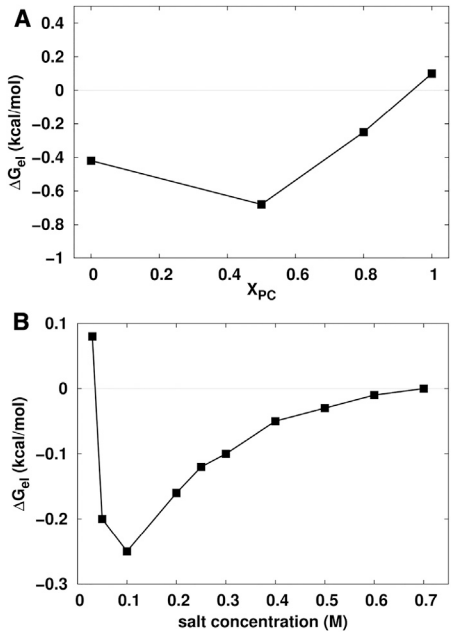

FIGURE 8 Influence of bilayer composition and salt concentration on the calculated electrostatic free energy. (*A*) The electrostatic free energy becomes more favorable as X_{PC} decreases from 1 to 0.5, and increases from $X_{PC} = 0.5$ to $X_{PC} = 0$. Calculations were done at 0.1 M KCl and with a protein-membrane distance of 3 Å (minimum ΔG_{el} in Fig. 7). (*B*) Electrostatic free energy as a function of salt concentration, which was varied from 0.025 to 0.7 M KCl ($X_{PC} = 0.8$). The protein is in the same position with respect to the bilayer in (*A*) and (*B*).

Affinity of *Bt*PI-PLC variants for SUVs

Using FCS, we determined the SUV binding affinities for a selection of *Bt*PI-PLC mutants that were chosen to test the computational predictions (Fig. 9; Table S8). K38, R71, and K279 are basic amino acids located in or close to the IBS of *Bt*PI-PLC. Their mutation to alanine does not significantly affect the protein structure (cf. Table S9) and they all show comparable enzymatic activity relative to the WT at $X_{PC} = 0.5$ (Fig. S4). Lower specific activity toward $X_{PC} = 0$ and 0.2 SUVs correlates with the loss of binding affinity provided by the removal of a given Lys or Arg (cf. Fig. S4 *B*).

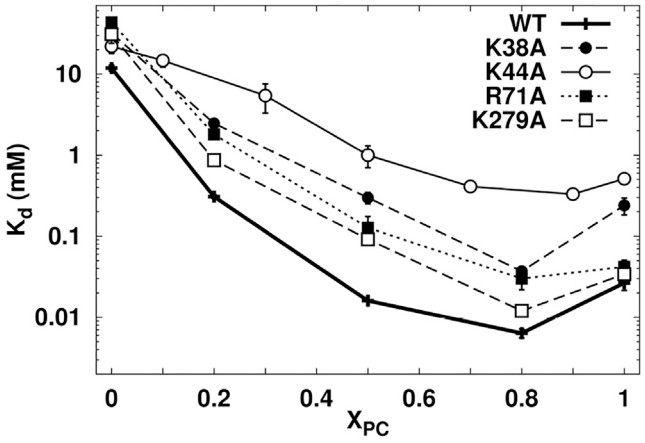

FIGURE 9 Binding of *Bt*PI-PLC WT and cationic amino acid variants to SUVs. The apparent K_d is plotted as a function of X_{PC}. Apparent K_d values are provided in Table S8.

Experiments measuring the affinity of the mutants for PC/PG SUVs show that R71A and K279A have apparent dissociation constants, K_d, that are 2–4 times higher than that of the WT toward SUVs containing $X_{PC} = 0$–0.5, and these mutants recover binding affinity at higher X_{PC} values, presumably due to the increased importance of specific tyrosine-mediated cation-π interactions with PC relative to electrostatics. The K38A mutation is more perturbing, with an ~10-fold lower K_d relative to the WT for 0.3–0.5 X_{PC} SUVs and little recovery of affinity at $X_{PC} = 1$, suggesting that this mutation may perturb more than nonspecific electrostatic interactions. However, none of these variants show the $\geq$2 orders of magnitude increases in K_d observed for K44A interactions with SUVs containing 0.1–0.9 X_{PC}. This result suggests that this cationic residue makes the largest contribution to the electrostatic interactions of the protein with the membrane. For SUVs with X_{PC} between 0.7 and 1.0, the K_d of K44A is relatively constant (0.4 $\pm$ 0.1 mM). The K_d of K44A toward pure PC SUVs is 20-fold higher than that of the WT. The simulations indicate that electrostatic interactions are unfavorable for WT binding to PC bilayers. Simulations with K44A also indicate that cation-π occupancies are not affected. However, a key protein-lipid hydrogen-bond network around helix B that interacts with DMPC phosphates is lost. The loss of these interactions could certainly account for the much higher than expected K_d of K44A for pure PC vesicles.

Distribution of basic amino acids in a database of peripheral membrane proteins

The low electrostatic partitioning combined with the major role of one particular basic residue is unexpected for a peripheral membrane protein. Our MD simulations and continuum electrostatic calculations indicate that this is due to the small number and spatial distribution of basic amino acids at the *Bt*PI-PLC IBS. To determine whether this feature of *Bt*PI-PLC is shared by other peripheral membrane proteins, we performed a statistical analysis on the predicted membrane orientations of proteins classified as peripheral/monotopic in the OPM database (31). The distribution of overall charges (Fig. 10 *A*) reveals that the balance of acidic and basic amino acids in these proteins does not show any overrepresentation of net positive charge. The mean density of basic amino acids on the protein surface seems to be slightly higher close to membrane headgroups (Fig. 10 *B*, where the phosphate density is expected to peak at insertion coordinates around −4 Å (34)). The distribution of the mean number of basic amino acids within 10 Å of the end of hydrocarbon region (Fig. 10 *C*) indicates that it is not uncommon for protein families in the data set to have three or fewer basic residues in this

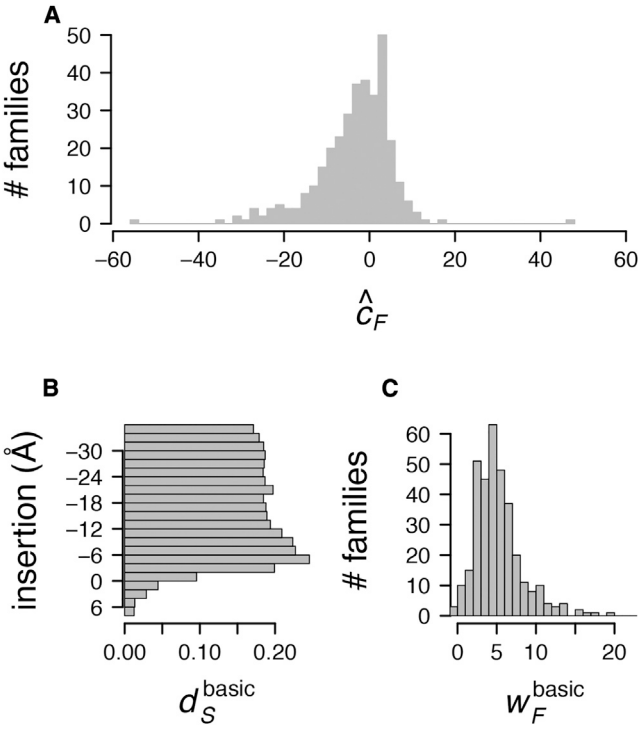

FIGURE 10 Peripheral membrane proteins often lack large basic patches. (*A*) Distribution of mean net charges ($\hat{c}_F$) for protein families in OPM. (*B*) Mean surface density of basic amino acids (d_S^{basic}) as a function of position along the membrane normal in predicted membrane-binding orientations from OPM. Positive values along the insertion axis correspond to the hydrocarbon region of the membrane. (*C*) Distribution of the mean number of basic amino acids close to the membrane (w_F^{basic}).

region. These results suggest that *Bt*PI-PLC is not unique, and that many peripheral membrane proteins may lack large surface clusters of basic amino acids.

DISCUSSION

Using computations, we have identified protein-lipid interactions (Figs. 5 and 7; Tables S3 and S7) that are in agreement with the membrane-affinity data obtained for *Bt*PI-PLC variants with tyrosine (Fig. S2) or basic amino acid mutations (Fig. 9). Using continuum electrostatic calculations, MD simulations, and FCS affinity measurements, we can thus formulate a complete model of *Bt*PI-PLC specific binding to anionic PC-containing vesicles. Weak nonspecific electrostatic interactions are dominated by Lys44, which upon mutation yields a loss of affinity resulting from the loss of not only nonspecific electrostatic interactions but also short-range interactions with bilayer lipids. The number of hydrogen bonds and hydrophobic contacts between the protein and lipids is not affected by the lipid composition. Instead, the balance between weak nonspecific electrostatics and opportunistic cation-π interactions ensures that the protein will interact preferentially with anionic vesicles containing large amounts of PC lipids.

Opportunistic choline-tyrosine cation-π interactions

Simulations of the enzyme at the interface of pure DMPG bilayers show a loose complex with a clear loss of short-range protein-lipid interactions, and in one of the MD replicas the protein dissociates from the bilayer after 200 ns. This result is particularly meaningful for a simulation started with the protein anchored at the bilayer interface, and is consistent with the weak vesicle affinity measured by FCS. On the other hand, the 500-ns-long MD simulations of *Bt*PI-PLC at the surface of mixed PC/PG bilayers result in a stably anchored protein. In agreement with previous experimental and computational studies, both helix B and the rim loop intercalate hydrophobic amino acids into the bilayers (7,8,35). However, neither hydrophobic contacts nor hydrogen bonds between the protein and lipids are dependent on the bilayer composition (cf. Table 1 and Fig. 5 *A*).

The simulations show that the occupancies of cation-π interactions between choline headgroups of DMPC and tyrosines vary as a function of DMPC content for the Tyr residues that make the largest contributions to membrane affinity (Y88, Y204, Y246, and Y251). Furthermore, the occupancies of these interactions during the simulations correlate qualitatively well with the effect their mutation has on the binding affinities of *Bt*PI-PLC (cf. Fig. S2): the higher the measured effect on the apparent K_d, the greater the occupancy of these interactions during the WT simulations. It is important to note that, unlike cation-π interactions observed in ligand-receptor binding (e.g., acetylcholine esterase (43) or histone tails (44)), *Bt*PI-PLC does not recruit choline groups to PC high-affinity binding sites. Rather, these interactions are opportunistic and occur stochastically in the presence of PC lipids. The opportunistic nature of these interactions might also explain the apparent saturation of cation-π interactions between Y246, Y251, and Y204 at high X_{PC}. The opportunistic character of the choline-protein interactions serves the function of *Bt*PI-PLC well, as it is a virulence factor that recognizes the extracellular leaflets of eukaryotic membranes, which have a high PC content.

Although the ability of CHARMM and other force fields to reproduce cation-π interactions between tryptophans and methylated lysines has been investigated (45), we are not aware of similar studies for interactions involving tyrosines. Even though our results cannot replace a systematic benchmark, they indicate that the force field provides a qualitatively satisfactory description of the tyrosine-choline interactions.

Unlike other basic amino acids, K44 is an interfacial residue

Another striking feature of *Bt*PI-PLC is the large effect that mutating a single lysine into an alanine has on the apparent

K_d. For vesicles with $X_{PC} = 0.8$, the mutation of K44 to alanine decreases the affinity ~55-fold compared with the WT or a contribution of 2.4 kcal/mol, which is clearly higher than the calculated electrostatic contribution (<1 kcal/mol). It is also higher than early reports of the contribution of basic amino acids to membrane binding. For example, Kim and co-workers (5) reported that the binding affinity of short basic peptides for vesicles containing acidic lipids was increased 10-fold by the introduction of each additional lysine, independently of the identity of the anionic lipid. This represents a contribution to the binding free energy of ~1.4 kcal/mol. Similarly, membrane targeting of the protein kinase pp60src (Src) and mutation of two of the six basic amino acids to neutral asparagines increased the K_d by 100, and mutation of five of the six increased the K_d by another order of magnitude. The latter is similar to the binding affinity of WT Src for neutral PC vesicles, showing that in that case, mutation of the basic cluster mainly affects the electrostatic interaction between Src and negatively charged vesicles (46). In addition, Wimley and White (47) reported a free energy of ~1 kcal/mol for the transfer of lysines to the interfacial region of POPC large unilamellar vesicles.

For *Bt*PI-PLC, the large effect of the K44A mutation is in agreement with what is expected from the computed transfer free energies of lysine and alanine side chains to the interface of a DOPC bilayer (48): −4.4 and −1.6 kcal/mol, respectively. The difference represents the cost of replacing the lysine by an alanine and amounts to 2.8 kcal/mol. Thus, the high contribution of Lys44 to membrane binding is due to its position in the headgroup region, where it participates in hydrophobic interactions with the lipid tails and long-lasting hydrogen bonds with lipid phosphate groups. K44 is located close to the average plane of the phosphate groups in the different bilayers, whereas other positively charged residues (i.e., K38, R71, and K279) are farther away from the IBS (Table S4). This also correlates with the moderate effects of the K38A, R71A, and K279A mutations on *Bt*PI-PLC affinity (Fig. 9).

Looking at the computed free energy of transfer of a lysine side chain through POPC bilayers as a function of the distance from the center of the membrane is very informative. The slope is rather steep along the 5–10 Å that separate the bulk from the preferred position of the charged side chain, with a difference between the two environments of ~2.5 kcal/mol (48–50). Thus, the contribution of basic amino acids at the IBS of peripheral membrane proteins will vary significantly depending on their position. The environment of these positive side chains and any intramolecular interactions they might engage in are also expected to modulate their contributions. Furthermore, our survey of the OPM database (31) shows that the distribution of surface basic amino acids in peripheral membrane proteins with respect to the membrane normal is rather broad (Fig. 10 *B*), indicating a potentially broad range of contributions of these amino acids to the affinity of peripheral membrane proteins for biological membranes. Thus, it is difficult to formulate a rule of thumb for the average contribution of each basic amino acid to peripheral membrane binding, since the magnitude of such contributions is context dependent.

Weak nonspecific electrostatic interactions

Our analyses of the simulations show that the short-range interactions that determine k_{off} do not explain *Bt*PI-PLC's specificity for PC vesicles containing negatively charged phospholipids. Therefore, we evaluated the interactions that contribute to k_{on} using continuum electrostatic methods, a qualitative approach that has proven reliable for that purpose. As expected, the calculated electrostatic contributions to *Bt*PI-PLC's association with bilayers depends on the anionic lipid content and is most favorable with equal amounts of zwitterionic and anionic lipids. It is less favorable for increasing amounts of PG anionic lipids. These results agree with the experimental data (42) and are due to unfavorable interactions between the large negative regions of the protein's surface potential and the anionic membrane. Despite an overall negative charge, *Bt*PI-PLC shows favorable electrostatic partitioning toward anionic membranes. In this respect, *Bt*PI-PLC is not unique, as other negatively charged amphitropic proteins are known to partition to anionic membranes (15). By contrast, a striking characteristic of *Bt*PI-PLC is the small magnitude of the electrostatic free energy ΔG_{el} (~−0.25 kcal/mol; Fig. 7) compared with what has been calculated for other peripheral membrane proteins using the same method (15,16). Although calculating ΔG_{el} using continuum electrostatic calculations has obvious limitations due to the simplicity of the model, comparisons of the *Bt*PI-PLC results with those obtained using the same approach for other proteins remain valid and informative. Furthermore, the affinity of *Bt*PI-PLC for neutral pure PC vesicles ($K_d = 0.026$ mM) is only ~4.1 times less favorable than that observed for vesicles with 20% anionic lipids ($K_d = 0.0064$ mM), which is the PC/PG ratio that yields the tightest binding (10). This corresponds to an electrostatic contribution of <1 kcal/mol. This value, like the computational evaluation, is significantly lower than reported experimental values for amphitropic proteins (~2 kcal/mol) (2). A marginally favorable ΔG_{el} means that the magnitude of the Coulombic contribution is only slightly higher than the magnitude of the desolvation penalty for the polar and charged residues (16). The low electrostatic interaction energy is explained by the absence of a well-defined cluster of basic amino acids at the *Bt*PI-PLC IBS (46,51).

Interestingly, a number of other membrane-binding peptides and proteins have been reported to have a low electrostatic partitioning. Amphipathic lipid-packing sensor motifs are short helical peptides found in proteins that target curved

membranes. Unlike many amphipathic helices, amphipathic lipid-packing sensor motifs have few basic amino acids and are described as weak electrostatic interactors with bilayers (52,53). It is thought that the lack of electrostatic interactions helps these peptides recognize membrane curvature. The human group X secreted phospholipase A_2 has been described as having an electrostatically neutral IBS. With just a few basic amino acids at the IBS, the continuum electrostatic calculations yield a slightly unfavorable ΔG_{el} (~0.30 kcal.mol^{-1}) when the protein is positioned next to the membrane. The same applies to the bee venom-secreted phospholipase A_2 ($\Delta G_{el} = 0.15$ kcal.mol^{-1}), which has been described as interfacially binding to membranes via a nonelectrostatic mechanism (54). The work presented here, along with the studies mentioned above, expands the literature on peripheral membrane proteins by highlighting a previously neglected class of peripheral membrane proteins that have weak electrostatic interactions with membranes.

Other peripheral membrane proteins display comparable distributions of basic amino acids

A survey of the peripheral proteins present in the OPM database allowed us to calculate and plot the net charges of membrane-binding proteins (Fig. 10 *A*). The resulting distribution of charges is comparable to what has been observed for the entire proteome of *Saccharomyces cerevisiae* (55) and indicates that peripheral membrane-binding proteins do not display a distribution of net charges skewed toward positive values. In fact, approximately one-third of the protein families classified as peripheral/monotopic in OPM have on average three or fewer basic amino acids within 10 Å of the membrane surface in their predicted membrane-bound state. It should be kept in mind that these charge estimates are based on simply counting basic and acidic residues, treating histidines as neutrally charged, and considering a neutral pH. Nonetheless, although some peripheral membrane proteins have strong electrostatic interactions with membranes, the results obtained from analyzing the OPM database suggest that weak nonspecific electrostatic interactors are less unusual among membrane-binding proteins than was previously thought.

CONCLUSIONS

Tyrosine-choline cation-π interactions are opportunistic and occur as the result of the presence of PC lipids in the membrane. We propose that they constitute a mechanism for the recognition of PC-rich eukaryotic cell membranes. The highest affinity of *Bt*PI-PLC toward slightly anionic SUVs is the result of weak electrostatic contributions from basic residues, particularly from one key basic residue. Our investigations show that the energetic contributions of basic amino acids to peripheral membrane binding are dependent on their position with respect to the IBS and how deep they might anchor in the lipid bilayer. As a result, and given the distribution of lysines and arginines in known amphitropic proteins, we suggest that weak nonspecific electrostatics might be more common than is generally thought and should be considered as a means for proteins to respond quickly to environmental changes.

SUPPORTING MATERIAL

Supporting Materials and Methods, four figures, and nine tables are available at http://www.biophysj.org/biophysj/supplemental/S0006-3495(16)00166-1.

AUTHOR CONTRIBUTIONS

H.M.K. performed the continuum electrostatic calculations and performed and analyzed the MD simulations with help from C.G. E.F. performed the statistical analysis of the OPM database. N.R. supervised the computational study. T.H. made all of the PI-PLC mutant proteins and characterized their enzymatic activity and biophysical properties. B.Y. helped with the FCS experiments. H.M.K., T.H., M.F.R., A.G., and N.R. designed the experiments. In addition, M.F.R. helped design mutations and supervised the biochemical characterization of the proteins. A.G. supervised the FCS experiments. N.R. wrote the manuscript, which was subsequently edited and approved by all of the authors.

ACKNOWLEDGMENTS

We thank the Norwegian metacenter for high-performance computing (NOTUR) for provision of CPU time.

This work was supported by grants from the Norwegian Research Council (FRIMEDBIO 214167 to N.R. and H.M.K.) and the National Institutes of Health (R01 GM060418 to M.F.R. and A.G.).

SUPPORTING CITATIONS

References (56–70) appear in the Supporting Material.

REFERENCES

1. Heimburg, T., and D. Marsh. 1996. Thermodynamics of the interaction of proteins with lipid membranes. *In* Biological Membranes: A Molecular Perspective from Computation and Experiments. K. M. Merz and B. Roux, editors. Birkhäuser Boston, Boston, pp. 405–462.
2. Johnson, J. E., and R. B. Cornell. 1999. Amphitropic proteins: regulation by reversible membrane interactions (review). *Mol. Membr. Biol.* 16:217–235.
3. Murray, D., A. Arbuzova, …, S. McLaughlin. 1999. Electrostatic properties of membranes containing acidic lipids and adsorbed basic peptides: theory and experiment. *Biophys. J.* 77:3176–3188.
4. Luckey, M. 2008. Membrane Structural Biology: With Biochemical and Biophysical Foundations. Cambridge University Press, Cambridge.
5. Kim, J., M. Mosior, …, S. McLaughlin. 1991. Binding of peptides with basic residues to membranes containing acidic phospholipids. *Biophys. J.* 60:135–148.
6. Pu, M., X. Fang, …, M. F. Roberts. 2009. Correlation of vesicle binding and phospholipid dynamics with phospholipase C activity: insights into phosphatidylcholine activation and surface dilution inhibition. *J. Biol. Chem.* 284:16099–16107.

7. Guo, S., X. Zhang, …, M. F. Roberts. 2008. Role of helix B residues in interfacial activation of a bacterial phosphatidylinositol-specific phospholipase C. *Biochemistry.* 47:4201–4210.
8. Grauffel, C., B. Yang, …, N. Reuter. 2013. Cation-π interactions as lipid-specific anchors for phosphatidylinositol-specific phospholipase C. *J. Am. Chem. Soc.* 135:5740–5750.
9. Yang, B., M. Pu, …, A. Gershenson. 2015. Quantifying transient interactions between *Bacillus* phosphatidylinositol-specific phospholipase-C and phosphatidylcholine-rich vesicles. *J. Am. Chem. Soc.* 137:14–17.
10. Pu, M., M. F. Roberts, and A. Gershenson. 2009. Fluorescence correlation spectroscopy of phosphatidylinositol-specific phospholipase C monitors the interplay of substrate and activator lipid binding. *Biochemistry.* 48:6835–6845.
11. Rhéault, J. F., È. Gagné, …, P. Lagüe. 2015. Molecular model of hemoglobin N from *Mycobacterium tuberculosis* bound to lipid bilayers: a combined spectroscopic and computational study. *Biochemistry.* 54:2073–2084.
12. Rogaski, B., and J. B. Klauda. 2012. Membrane-binding mechanism of a peripheral membrane protein through microsecond molecular dynamics simulations. *J. Mol. Biol.* 423:847–861.
13. Weber, D. K., S. Yao, …, F. Separovic. 2015. Characterization of the lipid-binding site of equinatoxin II by NMR and molecular dynamics simulation. *Biophys. J.* 108:1987–1996.
14. Busse, R. A., A. Scacioc, …, K. Kühnel. 2015. Characterization of PROPPIN-phosphoinositide binding and role of loop 6CD in PROPPIN-membrane binding. *Biophys. J.* 108:2223–2234.
15. Murray, D., S. McLaughlin, and B. Honig. 2001. The role of electrostatic interactions in the regulation of the membrane association of G protein beta gamma heterodimers. *J. Biol. Chem.* 276:45153–45159.
16. Mulgrew-Nesbitt, A., K. Diraviyam, …, D. Murray. 2006. The role of electrostatics in protein-membrane interactions. *Biochim. Biophys. Acta.* 1761:812–826.
17. Shi, X., C. Shao, …, M. F. Roberts. 2009. Modulation of *Bacillus thuringiensis* phosphatidylinositol-specific phospholipase C activity by mutations in the putative dimerization interface. *J. Biol. Chem.* 284:15607–15618.
18. Shao, C., X. Shi, …, M. F. Roberts. 2007. Dimer structure of an interfacially impaired phosphatidylinositol-specific phospholipase C. *J. Biol. Chem.* 282:9228–9235.
19. Humphrey, W., A. Dalke, and K. Schulten. 1996. VMD: visual molecular dynamics. *J. Mol. Graph.* 14:33–38, 27–28.
20. Kale, L., R. Skeel, …, K. Schulten. 1999. NAMD2: greater scalability for parallel molecular dynamics. *J. Comput. Phys.* 151:283–312.
21. Feller, S. E., Y. H. Zhang, …, B. R. Brooks. 1995. Constant pressure molecular dynamics simulation: the Langevin piston method. *J. Chem. Phys.* 103:4613–4621.
22. MacKerell, A. D., D. Bashford, …, M. Karplus. 1998. All-atom empirical potential for molecular modeling and dynamics studies of proteins. *J. Phys. Chem. B.* 102:3586–3616.
23. Mackerell, A. D., Jr., M. Feig, and C. L. Brooks, 3rd. 2004. Extending the treatment of backbone energetics in protein force fields: limitations of gas-phase quantum mechanics in reproducing protein conformational distributions in molecular dynamics simulations. *J. Comput. Chem.* 25:1400–1415.
24. Klauda, J. B., R. M. Venable, …, R. W. Pastor. 2010. Update of the CHARMM all-atom additive force field for lipids: validation on six lipid types. *J. Phys. Chem. B.* 114:7830–7843.
25. Brooks, B. R., C. L. Brooks, 3rd, …, M. Karplus. 2009. CHARMM: the biomolecular simulation program. *J. Comput. Chem.* 30:1545–1614.
26. Minoux, H., and C. Chipot. 1999. Cation-π interactions in proteins: can simple models provide an accurate description? *J. Am. Chem. Soc.* 121:10366–10372.
27. Baker, N. A., D. Sept, …, J. A. McCammon. 2001. Electrostatics of nanosystems: application to microtubules and the ribosome. *Proc. Natl. Acad. Sci. USA.* 98:10037–10041.
28. Sharp, K. A., and B. Honig. 1990. Calculating total electrostatic energies with the nonlinear Poisson-Boltzmann equation. *J. Phys. Chem.* 94:7684–7692.
29. Gallagher, K., and K. Sharp. 1998. Electrostatic contributions to heat capacity changes of DNA-ligand binding. *Biophys. J.* 75:769–776.
30. Singh, S. M., and D. Murray. 2003. Molecular modeling of the membrane targeting of phospholipase C pleckstrin homology domains. *Protein Sci.* 12:1934–1953.
31. Lomize, M. A., A. L. Lomize, …, H. I. Mosberg. 2006. OPM: orientations of proteins in membranes database. *Bioinformatics.* 22:623–625.
32. Hinsen, K. 2000. The molecular modeling toolkit: a new approach to molecular simulations. *J. Comput. Chem.* 21:79–85.
33. Miller, S., J. Janin, …, C. Chothia. 1987. Interior and surface of monomeric proteins. *J. Mol. Biol.* 196:641–656.
34. Lomize, A. L., I. D. Pogozheva, and H. I. Mosberg. 2011. Anisotropic solvent model of the lipid bilayer. 2. Energetics of insertion of small molecules, peptides, and proteins in membranes. *J. Chem. Inf. Model.* 51:930–946.
35. Feng, J., H. Wehbi, and M. F. Roberts. 2002. Role of tryptophan residues in interfacial binding of phosphatidylinositol-specific phospholipase C. *J. Biol. Chem.* 277:19867–19875.
36. Gasteiger, E., C. Hoogland, …, A. Bairoch. 2005. Protein identification and analysis tools on the ExPASY server. *In* The Proteomics Protocols Handbook. J. M. Walker, editor. Humana Press, New York, pp. 571–607.
37. Cheng, J., S. Karri, …, A. Gershenson. 2013. Does changing the predicted dynamics of a phospholipase C alter activity and membrane binding? *Biophys. J.* 104:185–195.
38. Schillinger, A. S., C. Grauffel, …, N. Reuter. 2014. Two homologous neutrophil serine proteases bind to POPC vesicles with different affinities: When aromatic amino acids matter. *Biochim. Biophys. Acta.* 1838:3191–3202.
39. Schrodinger, LLC. 2010. The PyMOL Molecular Graphics System, version 1.3r1.
40. Ben-Tal, N., B. Honig, …, S. McLaughlin. 1996. Binding of small basic peptides to membranes containing acidic lipids: theoretical models and experimental results. *Biophys. J.* 71:561–575.
41. Murray, D., and B. Honig. 2002. Electrostatic control of the membrane targeting of C2 domains. *Mol. Cell.* 9:145–154.
42. Wehbi, H., J. Feng, …, M. F. Roberts. 2003. Investigating the interfacial binding of bacterial phosphatidylinositol-specific phospholipase C. *Biochemistry.* 42:9374–9382.
43. Branduardi, D., F. L. Gervasio, …, M. Parrinello. 2005. The role of the peripheral anionic site and cation-π interactions in the ligand penetration of the human AChE gorge. *J. Am. Chem. Soc.* 127:9147–9155.
44. Lu, Z., J. Lai, and Y. Zhang. 2009. Importance of charge independent effects in readout of the trimethyllysine mark by HP1 chromodomain. *J. Am. Chem. Soc.* 131:14928–14931.
45. Zheng, X., C. Wu, …, G. R. Marshall. 2012. Molecular dynamics of β-hairpin models of epigenetic recognition motifs. *J. Am. Chem. Soc.* 134:15970–15978.
46. Sigal, C. T., W. Zhou, …, M. D. Resh. 1994. Amino-terminal basic residues of Src mediate membrane binding through electrostatic interaction with acidic phospholipids. *Proc. Natl. Acad. Sci. USA.* 91:12253–12257.
47. Wimley, W. C., and S. H. White. 1996. Experimentally determined hydrophobicity scale for proteins at membrane interfaces. *Nat. Struct. Biol.* 3:842–848.
48. MacCallum, J. L., W. F. Bennett, and D. P. Tieleman. 2007. Partitioning of amino acid side chains into lipid bilayers: results from computer simulations and comparison to experiment. *J. Gen. Physiol.* 129:371–377.
49. Bonhenry, D., M. Tarek, and F. Dehez. 2013. Effects of phospholipid composition on the transfer of a small cationic peptide across a model biological membrane. *J. Chem. Theory Comput.* 9:5675–5684.

50. MacCallum, J. L., W. F. Bennett, and D. P. Tieleman. 2008. Distribution of amino acids in a lipid bilayer from computer simulations. *Biophys. J.* 94:3393–3404.

51. McLaughlin, S., and A. Aderem. 1995. The myristoyl-electrostatic switch: a modulator of reversible protein-membrane interactions. *Trends Biochem. Sci.* 20:272–276.

52. Doucet, C. M., N. Esmery, …, B. Antonny. 2015. Membrane curvature sensing by amphipathic helices is modulated by the surrounding protein backbone. *PLoS One.* 10:e0137965.

53. Drin, G., J.-F. Casella, …, B. Antonny. 2007. A general amphipathic α-helical motif for sensing membrane curvature. *Nat. Struct. Mol. Biol.* 14:138–146.

54. Bollinger, J. G., K. Diraviyam, …, M. H. Gelb. 2004. Interfacial binding of bee venom secreted phospholipase A_2 to membranes occurs predominantly by a nonelectrostatic mechanism. *Biochemistry.* 43:13293–13304.

55. Ke, R., and S. Mitaku. 2005. Local repulsion in protein structures as revealed by a charge distribution analysis of all amino acid sequences from the *Saccharomyces cerevisiae* genome. *J. Phys. Condens. Matter.* 17:S2825–S2831.

56. Jo, S., T. Kim, …, W. Im. 2008. CHARMM-GUI: a web-based graphical user interface for CHARMM. *J. Comput. Chem.* 29:1859–1865.

57. Jorgensen, W. L., J. Chandrasekhar, …, M. L. Klein. 1983. Comparison of simple potential functions for simulating liquid water. *J. Chem. Phys.* 79:926–935.

58. Essmann, U., L. Perera, …, L. G. Pedersen. 1995. A smooth particle mesh Ewald method. *J. Chem. Phys.* 103:8577–8593.

59. Izaguirre, J. A., S. Reich, and R. D. Skeel. 1999. Longer time steps for molecular dynamics. *J. Chem. Phys.* 110:9853–9864.

60. Andersen, H. C. 1983. Rattle: a "velocity" version of the shake algorithm for molecular dynamics calculations. *J. Comput. Phys.* 52:24–34.

61. Venable, R. M., Y. Luo, …, R. W. Pastor. 2013. Simulations of anionic lipid membranes: development of interaction-specific ion parameters and validation using NMR data. *J. Phys. Chem. B.* 117:10183–10192.

62. Giorgino, T. 2014. Computing 1-D atomic densities in macromolecular simulations: the density profile tool for VMD. *Comput. Phys. Commun.* 185:317–322.

63. Gilson, M. K., and B. H. Honig. 1987. Calculation of electrostatic potentials in an enzyme active site. *Nature.* 330:84–86.

64. Middleton, E. R., and E. Rhoades. 2010. Effects of curvature and composition on α-synuclein binding to lipid vesicles. *Biophys. J.* 99:2279–2288.

65. Rusu, L., A. Gambhir, …, J. Rädler. 2004. Fluorescence correlation spectroscopy studies of Peptide and protein binding to phospholipid vesicles. *Biophys. J.* 87:1044–1053.

66. Thompson, N. L. 1991. Fluorescence correlation spectroscopy. *In* Topics in Fluorescence Spectroscopy. J. R. Lakowicz, editor. Plenum Press, New York, pp. 337–378.

67. Magde, D., E. L. Elson, and W. W. Webb. 1974. Fluorescence correlation spectroscopy. II. An experimental realization. *Biopolymers.* 13:29–61.

68. Elson, E. L., and D. Magde. 1974. Fluorescence correlation spectroscopy. 1. Conceptual basis and theory. *Biopolymers.* 13:1–27.

69. Murray, D., A. Arbuzova, …, S. McLaughlin. 2002. The role of electrostatic and nonpolar interactions in the association of peripheral proteins with membranes. *Curr. Top. Membr.* 52:277–298.

70. Lumb, C. N., and M. S. P. Sansom. 2012. Finding a needle in a haystack: the role of electrostatics in target lipid recognition by PH domains. *PLOS Comput. Biol.* 8:e1002617.

Biophysical Journal, Volume *110*

Supplemental Information

A Role for Weak Electrostatic Interactions in Peripheral Membrane Protein Binding

Hanif M. Khan, Tao He, Edvin Fuglebakk, Cédric Grauffel, Boqian Yang, Mary F. Roberts, Anne Gershenson, and Nathalie Reuter

Supporting Material for: A role for weak electrostatic interactions in peripheral membrane protein binding

Hanif M. Khan[1,2], Tao He[3], Edvin Fuglebakk[1,2], Cédric Grauffel[1,2], Boqian Yang[3,4], Mary F. Roberts[3], Anne Gershenson[4], Nathalie Reuter[1,2*]

[1] Department of Molecular Biology, University of Bergen, Bergen, Norway;
[2] Computational Biology Unit, Department of Informatics, University of Bergen, Bergen, Norway;
[3] Department of Chemistry, Boston College, Chestnut Hill, U.S.A.;
[4] Department of Biochemistry and Molecular Biology, University of Massachusetts, Amherst, U.S.A.

[*] Corresponding Author- NR: Universitetet i Bergen, Computational Biology Unit, Institutt for informatikk, Pb. 7803 N-5020 Bergen, nathalie.reuter@uib.no.

Methods.

Bilayer preparation for MD simulations

Bilayers of DMPC, DMPG and DMPC:DMPG lipid mixtures were built using the CHARMM-GUI (1). We considered four bilayers: pure DMPC (X_{PC} = 1.0), a 80:20 (X_{PC} = 0.8) mixed bilayer, a 50:50 (X_{PC} = 0.5) mixed bilayer, and pure DMPG (X_{PC} = 0). Where X_{PC} represents the mole fraction of PC lipids in the mixture. All bilayers contain 256 lipids (128 in each leaflet). TIP3P (2) water molecules were added to hydrate the lipids and sodium was used as a counter-ion to achieve overall charge neutrality of the system when necessary. The CHARMM36 force field, with updates for lipids (3), and NAMD (v2.9) (4) were used for the simulations. The bilayers were first minimized using 4000 steps of a conjugate gradient algorithm. The system was then equilibrated at 310 K, and 1 atm in the NPT ensemble for 400 ps with constant area in the x-y dimension and 2 fs time steps. The temperature was controlled with Langevin dynamics with the temperature damping coefficient set to 1.0 and the velocities periodically reassigned every 1 ps. The pressure was controlled using the Langevin piston method (5) with an oscillation period of 75 fs and a damping time scale of 25 fs. We used anisotropic pressure coupling. The non-bonded interactions cut-off was set to 12 Å and long-range electrostatics corrections beyond the cut-off were modeled using the Particle Mesh Ewald (6) method. We used switching functions for both the electrostatics and van der Waals interactions with the switch distance set to 11 Å. We used the r-RESPA (7) multiple time step algorithm and short-range non-bonded forces were evaluated every 2 fs while long-range electrostatics were evaluated every 4 fs. SHAKE (8) was used to constraint all bonds between hydrogen atoms and heavy atoms. The systems were then further equilibrated for 200 ps after removing the constant area constraint. The bilayers were further simulated for 100 ns in the NPT ensemble without velocity reassignment. The bilayer with a 50:50 PC:PG ratio (X_{PC} = 0.5) was simulated for 200 ns to achieve proper lipid mixing. The pressure control parameters for the Langevin piston method were altered to 200 fs for the oscillation period and 50 fs for the damping time scale. All other simulation parameters remained unchanged. The areas per lipid for all of the bilayers are listed in Table S1.

We did not use a correction for the Lennard Jones potential between Na^+ and lipid oxygens (9) for several reasons. Since our simulations start with the protein inserted in the bilayer, we do not expect the ions to play a significant role in the protein-bilayer interaction as indicated by the low electrostatic partitioning (Cf. Results section, continuum electrostatics calculations), and to our knowledge the correction has not been benchmarked on systems containing surface-bound proteins or peptides. We did prepare a DMPG bilayer using the Lennard-Jones correction though, and then ran test simulations with *Bt*PI-PLC using the correction. Under these conditions, *Bt*PI-PLC binding to the bilayer was unstable as we also observed in the simulations without the NBFIX correction.

Minimization of the protein-bilayer systems

Subsequent to the docking of the protein onto the bilayer, membrane and protein were submitted to an energy minimization using the following harmonic restraints: 150 kcal/mol/Å^2 for the protein backbone and water molecules; 100 kcal/mol/Å^2 for membrane atoms located further than 5 Å from the protein and protein side chain atoms located further than 5 Å from the membrane; 50 kcal/mol/Å^2 for membrane atoms located within 5 Å of the protein; 15 kcal/mol/Å^2 for protein side chains atoms located 5 Å or less from the membrane. The minimization consisted of 20 consecutive cycles of 600 minimization steps (500 steepest descents, 100 conjugated gradients) with the restraints scaled by 0.65 after each cycle.

MD trajectory analysis

All analyses were performed on the last 450 ns of each simulation using CHARMM (v33b1) (10) and VMD (v1.9.1) (11). Hydrophobic interactions between the protein and lipid bilayer were assigned if the protein and membrane candidate atoms were within 3 Å of each other for at least 10 ps. For the protein, candidate atoms for hydrophobic contacts are side chain atoms from aliphatic and aromatic groups, while for the lipid bilayer; the candidate atoms are from the hydrophobic lipid tails. Hydrogen bonds were assigned using the donor and acceptor definitions from the CHARMM (12) force field with a distance cut-off of 2.4 Å and an angle cut-off of 130 degrees. The two cut-off criteria had to be met for at least 10 ps. Cation-π interactions between the aromatic amino acids (Tyr, Phe and Trp) and the choline group of the DMPC lipids were assigned if the nitrogen atom of the choline group was within 7 Å of the aromatic rings. Additionally these distances should not vary more than 1.5 Å (13, 14). Combining these two criteria, we can screen for the possible formation of cation-π adducts during the course of simulation. Hydrophobic contacts, hydrogen bonds and cation-π interactions are averaged over the two replicas.

Occupancy of a particular interaction is reported as the number of conformations with the interaction present divided by the total number of conformations in the trajectory sampling window.

Electron density profiles (EDP) were generated using the Density Profile Tool (15) VMD plugin. EDPs were calculated from the trajectory at 1 ns intervals. The projection axis is the z-axis, which is also the bilayer normal. The profile resolution is $\Delta z = 1$ Å for the protein and lipid bilayer. The profile resolution is $\Delta z = 0.5$ Å for helix B and phosphate planes of the membrane.

Continuum electrostatics calculations

Poisson-Boltzmann calculations are carried out using APBS (version 1.3) (16). The parameters for protein and ions are adapted from the CHARMM all atom force field (c22 including CMAP correction) (17) and for the lipids from the force field update for lipids (Charmm36) (3). The non-linear Poisson-Boltzmann equation is solved using the focusing technique (18). Coarse grid dimensions are expanded by a factor of 2.5 as both

*Bt*PI-PLC and anionic membranes are highly charged. Fine grid dimensions are obtained by adding 50 Å to the molecular dimensions. We used a fine grid spacing of 0.5 or 0.35 Å. The difference in the calculated electrostatic free energy was less than 0.003 kcal/mol; therefore a fine mesh spacing of 0.35 Å was chosen for all of the calculations. The solute dielectric is set to 2 and the solvent (water) dielectric is set to 80. KCl is used to investigate the effects of salt concentration on the electrostatics.

The electrostatic free energy for the protein, $G_{el}(P)$, the membrane, $G_{el}(M)$, and the protein membrane complex, $G_{el}(P.M)$, were all calculated. The electrostatic free energy contribution to the free energy of binding due to protein membrane interactions can then be evaluated as follows:

$$\Delta G_{el} = G_{el}(P.M) - [G_{el}(P) + G_{el}(M)] \qquad \text{(S1)}$$

Database statistics

Analysis of net charges For the selected families, we obtained average net charges, $\hat{c}_F$, for each family, *F*, as:

$$\hat{c}_F = \frac{1}{|F|}\sum_{p\in F} c_p \qquad \text{(S2)}$$

where $|F|$ is the number of proteins in the family *F*, and c_p is the net charge of a protein obtained as:

$$c_p = K_p + R_p - E_p - D_p \qquad \text{(S3)}$$

where K_p, R_p, E_p, and D_p respectively denote the number of lysines, arginines, glutamates and aspartates in the protein.

Analysis of basic residues For a family F, we calculated the mean number of basic amino acids at the IBS as:

$$w_F^{\text{basic}} = \frac{1}{|F|}\sum_{p\in F} n_p^{\text{basic}}\left(0, -10\text{Å}\right) \qquad \text{(S4)}$$

where 'basic' denote amino acids of type Lys or Arg. Please note that the plot in Figure 10 has been truncated to exclude one family with $w_F^{\text{basic}} > 40$.

We also calculated the mean surface density of basic amino acids at varying distances from the membrane. We define this statistic for windows of size *l* around different insertion coordinates. For a family *F*, the mean surface density of basic amino acids is:

$$d_F^{\text{basic}}(i,l) = \frac{1}{|F|}\sum_{p\in F} \frac{n_p^{\text{basic}}\left(i-\frac{l}{2}, i+\frac{l}{2}\right)}{n_p^{\text{any}}\left(i-\frac{l}{2}, i+\frac{l}{2}\right)} \qquad \text{(S5)}$$

where 'any' denotes amino acids of any type. We report averages over the entire dataset:

$$d_S^{\text{basic}} = \frac{1}{|S|}\sum_{F\in S} d_F^{\text{basic}}(\text{i}, 2\text{Å}) \qquad \text{(S6)}$$

where $|S|$ denotes the number of families in the set.

FCS measurements of BtPI-PLC binding to SUVs

FCS experiments were carried out at 22 ^{o}C on 300 μL samples in phosphate buffered saline (PBS), pH 7.4, plus 1 mg/ml BSA to stabilize *Bt*PI-PLC, in chambered coverglass wells (LabTek). The wells were coated with 10 mg/ml BSA and rinsed with PBS prior to use to prevent protein adhesion to the sides of the wells. 10 nM labeled PI-PLC was titrated with SUVs, and the fraction of protein bound to vesicles was determined from two species fits to the autocorrelation, $G(\tau)$, (obtained in crosscorrelation mode) as described previously (19). In brief:

$$G(\tau) = A_p g_p(\tau) + A_v g_v(\tau) \qquad \text{(S7)}$$

where p and v denote free protein and SUVs that are fluorescent due to PI-PLC binding, respectively, and A_j is the amplitude of species j (19-22). The correlation function for species j, $g_j(\tau)$, accounts for translational diffusion of the molecules through the observation volume. The measured diffusion times depend on the radius and extent of the observation volume, determined from fits to rhodamine 110 calibration data using D = 280 $\mu m^2 s^{-1}$ at 22 ^{o}C (23), and D_j, the diffusion coefficient for each species (22, 24). D_p for the free protein was experimentally determined in the absence of vesicles while D_v for the SUVs was determined from global fits to all of the titration experiments for a particular X_{PC} using Origin (OriginLab). The apparent fraction of protein bound to the SUVs, *f*, can be determined from A_p and the time-averaged number of proteins in the observation volume in the absence of vesicles <No>, by:

$$f = 1\text{-}A_p\langle N_o\rangle = 1\text{-}A_p/A_{p,o} \qquad \text{(S8)}$$

where $A_{p,o}=1/\langle N_o\rangle$ is the autocorrelation amplitude for free *Bt*PI-PLC prior to vesicle titrations and corrected for volume changes. The apparent dissociation constant, K_d, representing *Bt*PI-PLC partitioning onto the vesicle, and a cooperativity coefficient, *n*, were determined from fits to the equation:

$$f = f_{max}\,[PL]^n/(K_d^n+[PL]^n) \qquad \text{(S9)}$$

where *f*, is determined for different total lipid concentrations, [PL], at fixed X_{PC}, and f_{max} is the apparent maximum fraction bound. FCS experiments were repeated twice using different vesicle and protein preparations. Assuming that uncertainties are normally distributed and considering the range of standard deviation values from all of the FCS measurements, a 2-3 times increase in apparent K_d relative to N168C PI-PLC (WT*) is considered significant.

Table S1. Area per lipid for different bilayers obtained from MD simulations.

X_{PC}	Area per lipid ($Å^2$)
1.0	60.9±0.9
0.8	59.6±0.9
0.5	58.5±1.0
0.0	59.1±1.0

Table S2. Average RMSD (with standard deviation) of the *Bt*PI-PLC backbone along the MD simulations relative to the starting protein structure (minimized X-ray crystal structure in the presence of the bilayer).

X_{PC}	replicate	RMSD (Å)
1.0	r1	1.44±0.11
	r2	1.34±0.12
0.8	r1	1.43±0.10
	r2	1.17±0.11
0.5	r1	1.43±0.13
	r2	1.61±0.09

Table S3. Inventory of interactions between *Bt*PI-PLC and the bilayers[a].

SSE[b]	aa	Hydrophobic [c]			Hbonds (%) [d]			Cation-π (%) [e]		
		X_{PC}			X_{PC}			X_{PC}		
		0.5	0.8	1	0.5	0.8	1	0.5	0.8	1
αB	Q40	1.8	2.5	2.4	**64.4**	**99.2**	**92.0**			
	N41	1.1	1.5	1.4	**62.5**	**96.8**	**90.5**			
	P42	4.9	5.8	5.6						
	I43	8.6	7.8	7.8						
	K44	3.3	1.4	2.3	85.9	98.3	98.5			
	Q45				19.7	27.2	33.3			
	V46	3.6	4.5	4.2						
	W47	2.9	2.2	2.6				23.4	12.5	3.3
	Y53							1.6	8.1	1.9
β2	R71				49.4	50.5	38.7			
β2-αD	P84	4.9	2.6	2.7						
	L85	3.4	1.2	2.3						
	Y86							9.9	15.6	11.9
	Y88				42.2	58.0	61.6	33.8	55.6	93.1
β3-αE	Y118							1.6	7.8	12.9
	K122				67.8	56.2	56.9			
β6-αF	Y200							49.8	12.1	43.0
	K201				53.7	46.5	45.0			
αF	Y204							18.0	25.5	22.3
β7-αG	S236				38.5	33.4	32.8			
	G238	0.8	0.9	1.1						
	G239	0.9	1.9	2.3						
	T240	2.7	2.5	2.6						
	A241	3.2	3.1	3.2						
	W242	2.9	2.8	2.9						
	S244				43.0	82.0	68.4			
αG	Y246				20.1	12.9	34.6	50.1	84.5	80.9
	Y247				29.2	36.0	43.7	11.1	11.9	12.7
	Y251				35.6	34.0	38.8	31.7	47.4	47.0

[a] DMPG simulations (X_{PC}=0) are not included as (1) they do not show tight binding of the protein, and (2) we want to follow the dependence of the interactions on the PC:PG ratio (some interactions such as cation-π obviously disappear in the absence of PC). The results presented in the table above are averages over two replicas using the last 450ns of each simulation. [b] Secondary structure elements; α: helix, β: strand, βi-αX: loop between strand i and helix X. [c] Average number of hydrophobic contacts per frame. [d] Occupancies of hydrogen bonds in %. Only the hydrogen bonds observed in the two replicas at the same X_{PC} are shown. Hydrogen bonds reported are mainly between the lipid phosphate groups and amino acid side chains but a few hydrogen bonds form with the protein backbone (**bold numbers**). Hydrogen bonds with headgroups or glycerol groups are not stable throughout the simulations. [e] Occupancies of cation-π adducts.

Table S4. Simulation averages of the anchoring depth of *Bt*PI-PLC residues in the bilayer. Positive values indicate that the centers of mass of the amino acids are on average buried below the phosphate group of the lipids during the simulation. The average phosphate plane is used as the reference plane.

SSE	aa	X_{PC} = 1.0		X_{PC} = 0.8		X_{PC} = 0.5		X_{PC} = 0
		r1	r2	r1	r2	r1	r2	r1
β1-αB	K38	-6.8±2.2	-7.6±2.3	-8.1±2.0	-6.7±2.5	-6.8±3.1	-9.3±3.1	-8.4±3.0
αB	Q40	0.6±2.3	-0.2±2.4	-1.1±2.1	-0.4±2.5	0.5±3.3	-2.8±3.1	-2.0±3.1
	N41	3.3±1.8	2.8±2.0	2.3±1.7	3.4±2.3	3.1±2.4	0.7±2.4	1.3±2.6
	P42	4.2±1.9	3.7±1.9	3.0±1.8	4.0±2.2	3.8±2.5	1.5±2.3	1.7±2.7
	I43	4.3±1.7	3.9±1.8	3.7±1.6	4.3±2.1	4.2±1.9	2.5±1.8	2.3±2.4
	K44	0.4±1.7	-0.2±1.8	-0.3±1.6	0.5±2.2	0.4±1.9	-1.1±1.8	-1.3±2.3
	Q45	-0.6±1.9	-1.0±1.9	-1.8±1.8	-0.8±2.1	-1.0±2.4	-3.3±2.0	-3.1±2.7
	V46	0.4±1.9	0.3±1.8	-0.3±1.7	0.3±2.0	0.3±1.9	-2.1±1.9	-1.8±2.7
	W47	-0.8±1.9	-0.7±2.2	-0.7±1.9	-0.8±2.1	0.1±1.7	-2.3±1.8	-2.6±2.6
β2	R71	-10.1±2.0	-10.9±2.4	-10.0±2.3	-9.1±3.1	-9.6±1.8	-10.2±2.3	-10.3±2.5
β2-αD	P84	-3.2±1.9	-4.5±2.3	-2.5±2.0	-2.2±2.7	-1.3±1.6	-3.8±1.7	-4.0±2.4
	L85	-3.6±1.6	-4.2±2.0	-3.7±1.7	-2.9±2.4	-2.9±1.7	-4.8±1.7	-4.7±2.3
	Y86	-5.5±1.9	-7.0±2.2	-6.1±1.9	-5.0±2.8	-2.0±2.1	-6.8±2.5	-6.7±2.4
	Y88	-4.9±2.0	-5.8±2.3	-5.9±2.0	-4.4±2.6	-6.3±2.4	-6.4±3.0	-6.2±2.7
β3-αE	Y118	-8.7±2.1	-8.1±2.6	-8.2±2.3	-7.4±3.1	-8.3±1.8	-7.0±2.2	-7.9±2.7
	K122	-6.1±2.9	-5.3±3.3	-5.2±3.3	-5.1±4.2	-5.0±2.5	-5.3±3.0	-5.8±3.2
β6-αF	Y200	-10.9±2.2	-10.8±2.5	-10.4±1.8	-10.7±2.5	-10.5±2.2	-11.8±3.3	-12.2±4.2
	K201	-7.6±2.6	-7.5±2.8	-7.2±2.1	-7.4±2.8	-7.0±2.6	-8.7±4.0	-9.7±4.4
αF	Y204	-7.3±2.6	-7.5±2.5	-8.3±2.7	-8.6±2.5	-8.7±2.8	-11.6±4.1	-12.6±4.0
β7-αG	S236	-6.6±2.0	-6.5±2.2	-6.1±1.8	-6.5±2.2	-6.4±2.0	-7.8±3.1	-8.9±3.6
	S237	-3.0±1.9	-3.0±2.1	-2.8±1.8	-2.9±2.1	-2.7±1.9	-5.5±3.9	-5.6±3.8
	G238	0.1±2.0	0.2±2.2	0.4±1.8	0.0±2.3	0.4±2.1	-2.5±3.6	-3.8±4.2
	G239	2.2±1.9	2.1±2.0	2.2±1.7	2.2±2.1	2.4±2.0	0.3±3.1	-1.4±4.2
	T240	3.3±2.0	3.3±2.0	2.9±1.9	3.0±2.0	3.1±2.2	1.2±3.1	-0.8±3.5
	A241	2.6±2.2	2.5±1.9	1.7±2.1	2.0±2.1	2.0±2.5	0.4±2.6	0.1±3.3
	W242	3.9±2.4	4.1±2.1	3.3±2.2	3.3±2.2	3.3±2.4	1.3±3.3	3.1±3.2
	N243	-0.3±2.3	0.0±2.1	-0.4±2.0	-0.6±2.2	-0.5±2.3	-2.5±3.4	-2.0±3.4
	S244	-2.3±2.1	-2.3±1.9	-2.9±1.9	-2.7±2.0	-2.7±2.2	-4.4±2.6	-4.4±3.2
αG	Y246	-4.5±2.4	-4.3±2.1	-6.0±2.2	-5.2±2.2	-5.4±2.5	-8.2±2.4	-8.8±3.1
	Y247	-2.3±2.5	-2.0±2.2	-3.4±2.4	-3.2±2.2	-3.2±2.5	-5.5±2.9	-6.1±3.6
	S250	-7.2±2.7	-6.9±2.4	-8.7±2.5	-8.1±2.4	-8.3±2.7	-11.3±2.9	-11.7±3.4
	Y251	-6.7±3.2	-5.8±2.5	-7.6±2.7	-7.4±2.6	-7.2±2.9	-10.3±3.7	-10.9±4.0
β8-αH	K279	-8.1±3.1	-8.1±3.0	-10.1±2.9	-9.3±3.1	-9.5±3.6	-12.6±2.9	-12.7±3.5

Table S5. Number of DMPC lipids mediating one or more cation-π interactions with *Bt*PI-PLC tyrosines (mixed bilayer, X_{PC} = 0.5).

Residue	Replica 1	Replica 2
Y251	4	5
Y246	2	2
Y88	1	2

Table S6. Occupancies of Y251 cation-π interactions involving more than one PC lipid simultaneously. The occupancies (%) are reported for the three different PC bilayer compositions. Reported replicates are chosen based on the presence of cation-π interactions between Y251 and more than one lipid.

X_{PC} & replica	Occupancies (%)
X_{PC} = 1 r2	11.5
X_{PC} = 0.8 r1	11.1
X_{PC} = 0.5 r1	4.8

Table S7. Anchorage depth and inventory of interactions for *Bt*PI-PLC K44A and a mixed bilayer (X_{PC}=0.8).

SSE	aa	depth (Å)	Hydrophobic	Hbonds (%)[a]	Cation-π (%)
αB	Q40	-1.4±1.9	0.9	**7.2**[b]/34.6	
	N41	1.8±1.7	0.5	**7.2**/17.0/9.8[c]	
	P42	2.9±1.6	5.2		
	I43	3.4±1.6	8.2		
	K44A	-0.9±1.6	1.6		
	Q45	-1.9±1.6	0.3	18.5	
	V46	-0.3±1.6	3.9		
	W47	-0.2±1.6	4.1		
β2	R69	-12.3±1.7		80.6	
	R71	-9.4±2.2		73.4	
β2-αD	H82	-7.4±1.7	1.1	6.6	
	P84	-2.2±2.0	6.3		
	L85	-3.3±1.7	5.0		
	Y86	-6.4±2.5		**22.9**/9.3	14.7
	Y88	-6.6±2.2		63.7	38.2
β3-αE	Y118	-7.4±2.3		35.1	36.0
	K122	-8.0±4.0		**7.9**/26.3	
β6-αF	Y200	-9.8±2.1			93.1
	K201	-6.3±2.4		63.8	
αF	N203	-6.5±3.0		12.4	
	Y204	-8.4±2.9		6.9	32.4
β7-αG	S236	-6.7±1.8	0.3	22.9	
	S237	-3.1±1.8			
	G238	0.1±1.9	1.4		
	G239	1.9±1.8	0.5		
	T240	2.6±2.0	2.5		
	A241	1.2±2.1	3.2		
	W242	2.8±2.3	2.7	12.6/11.2[d]	
	N243	-0.8±2.2		16.3	
	S244	-3.4±1.9		79.5	
αG	Y246	-6.3±2.1		8.1	85.7
	Y247	-3.8±2.4		43.5	13.3
	Y248	-6.5±2.2			
	S250	-9.3±2.4			
	Y251	-8.1±2.8		34.2	50.3

[a] Hbonds occur mainly between sidechains and phosphate groups; [b] Hbond between backbone and phosphate (bold numbers) [c] Hbond between sidechain and headgroup; [d] Hbond between sidechain and glycerol

Table S8. Binding affinities of *Bt*PI-PLC variants for PC/PG SUVs.

	Apparent K_d (mM)				
*Bt*PI-PLC [a]	X_{PC} = 0	0.2	0.5	0.8	1.0
WT	12±1	0.31±0.01	0.016±0.001	0.0064±0.0008	0.026±0.005
K38A	32±1	2.2±0.2	0.30±0.05	0.037±0.002	0.024±0.06
K44A	22±4	8.8 [b]	1.0±0.3	0.35 [b]	0.51±0.07
R71A	43±5	1.8±0.2	0.13±0.05	0.030±0.008	0.042±0.009
K279A	31±7	0.87±0.04	0.092±0.011	0.012±0.002	0.034±0.008

[a] All of the *Bt*PI-PLC variants contain the N168C mutation for fluorescent labeling
[b] Data for K44A binding at X_{PC}=0.2 and 0.8 was interpolated from data between X_{PC} = 0.1 and 0.3 and X_{PC} = 0.7 and 0.9, respectively.

The measured apparent K_d values for K44A are:

X_{PC}	Apparent K_d (mM)
0	22.2±3.9
0.1	14.7±2.5
0.3	5.43±2.13
0.5	1.03±0.28
0.7	0.41±0.06
0.9	0.33±0.03
1.0	0.51±0.07

Table S9. Comparison of secondary structure content and T_m values for WT and mutant *Bt*PI-PLCs from far UV circular dichroism (CD) data.

Protein	% Secondary Structure				T_m (^oC)[a]
	α-Helix	*β*-Sheet	*β*-Turn	Random Coil	
WT	21	32	17	30	57.1
K38A	20	33	17	30	57.3
K44A	22	31	17	30	60.3
R71A	21	31	17	30	56.8
K279A	21	32	17	30	56.0

[a] Loss of secondary structure was assessed by monitoring the ellipticity at 222 nm as a function of temperature

Figure S1. The β7-αG loop is more flexible in simulations without PC lipids. The RMSD of the loop relative to **its initial conformation** is plotted across the simulations for *Bt*PI-PLC interacting with lipid bilayers with different lipid compositions. On a pure DMPG bilayer (X_{PC} = 0, black) the loop loses intramolecular interactions resulting in more flexibility.

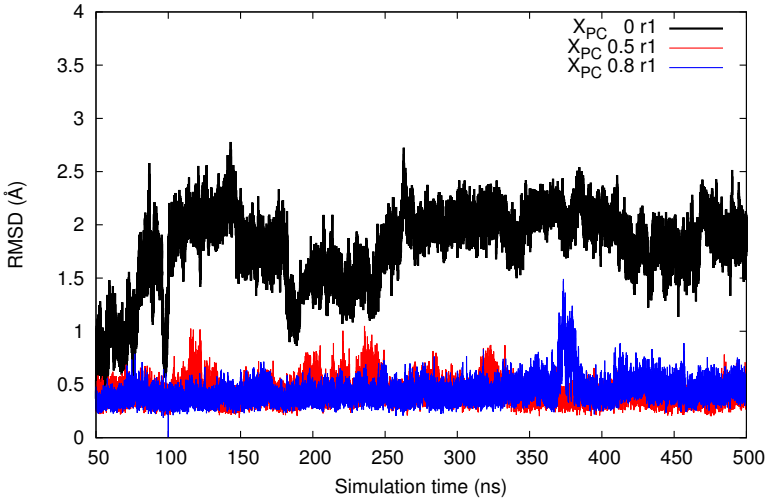

Figure S2. Comparison between occupancies of cation-π interactions observed during the MD simulations and evaluation of ΔΔG calculated from apparent K_d values measured by FCS for *Bt*PI-PLC WT and single tyrosine mutant at X_{PC}=1.0 (A), 0.8 (B) and 0.5 (C). K_d value are from *Grauffel et al*. (13). See this reference for an explanation of the role of Y248 and the effect of mutating this tyrosine to alanine.

A

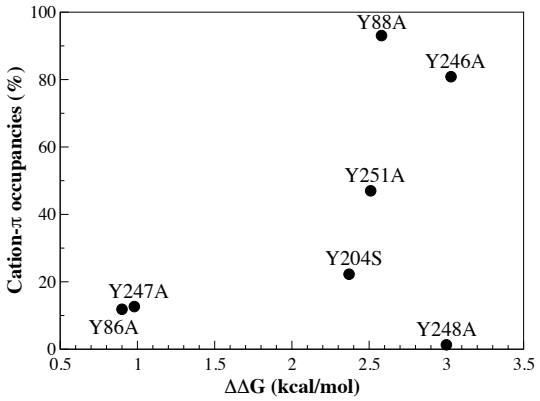

B

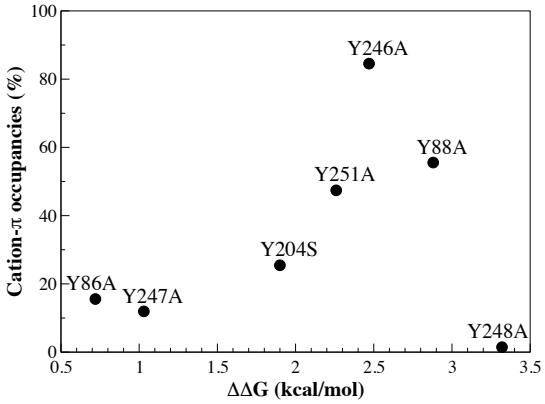

C

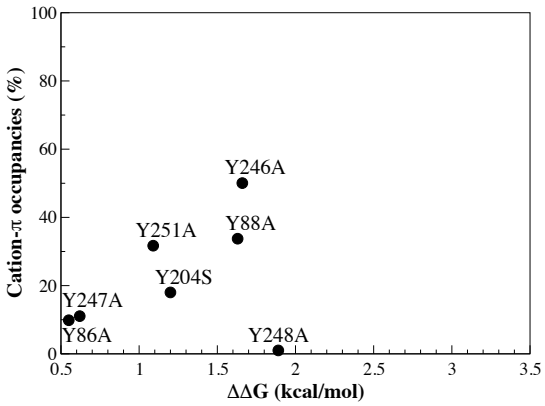

Figure S3. Calculated electrostatic potential of the *Bt*PI-PLC-membrane complex (X_{PC}=0.8) when *Bt*PI-PLC is 4 Å above the membrane. Isocontours of -/+ 1 (unit k_BT/e) are mapped on the molecular surface (negative: red; positive: blue). (A) Side view, in an equilibrated bilayer isosurfaces are not essentially flat. (This contrasts with other published views where isosurfaces for model membranes are represented as flat (25-27)) (B) Top view, local zones of blue and red alternate in the membrane. This pattern is also observed for a zwitterionic membrane (POPC/DMPC) (28).

A **B**

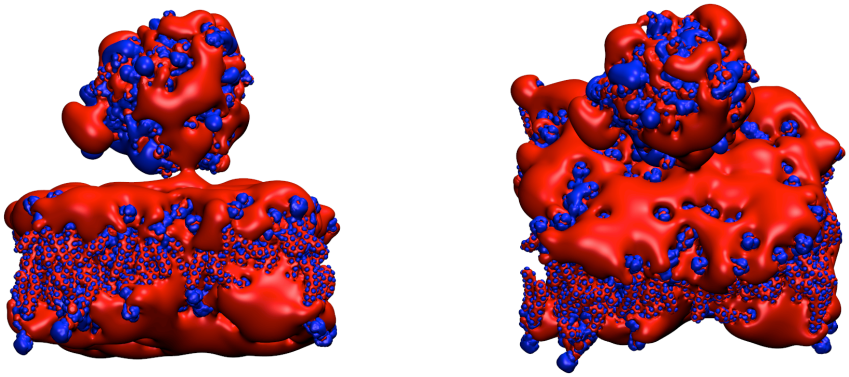

Figure S4. Specific activity of *Bt*PI-PLC variants towards PI/POPC SUVs with 2 mM PI and varying X_{PC}: WT (solid circle), K38A (open circle), K44A (solid square), R71A (inverted triangle), and K279A (triangle). Protein concentrations were adjusted to between 0.15-2 μg/ml to ensure less than 20% cleavage of the PI. The specific activity is given in μmol/(min*mg enzyme). A) All cationic residue mutants exhibit enzymatic activity similar to wildtype (WT) for $X_{PC} \geq 0.5$ implying that the active site is not significantly perturbed in these alanine mutants. (B) A zoomed in view of the activity for low X_{PC}. i.e., more anionic SUVs, showing the extremely low activity of K44A.

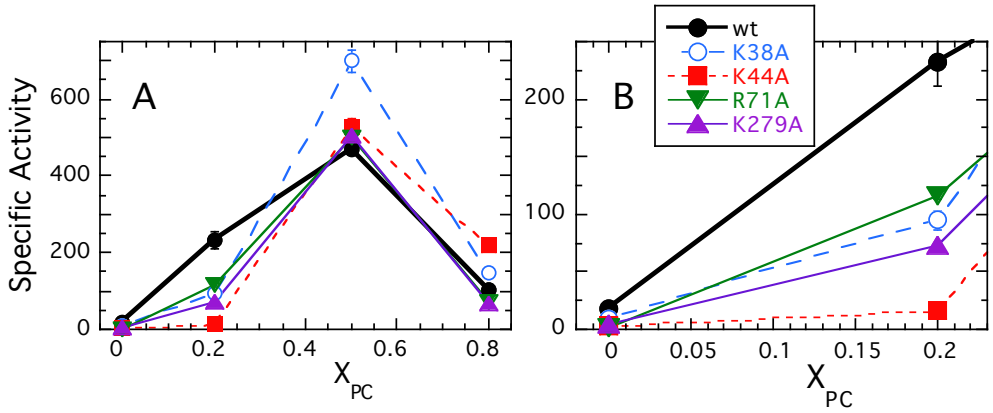

SUPPORTING REFERENCES

1. Jo, S., T. Kim, V. G. Iyer, and W. Im. 2008. CHARMM-GUI: A web-based graphical user interface for CHARMM. J Comput Chem 29:1859-1865.
2. Jorgensen, W. L., J. Chandrasekhar, J. D. Madura, R. W. Impey, and M. L. Klein. 1983. Comparison of simple potential functions for simulating liquid water. J Chem Phys 79:926-935.
3. Klauda, J. B., R. M. Venable, J. A. Freites, J. W. O'Connor, D. J. Tobias, C. Mondragon-Ramirez, I. Vorobyov, A. D. MacKerell, Jr., and R. W. Pastor. 2010. Update of the CHARMM all-atom additive force field for lipids: validation on six lipid types. J Phys Chem B 114:7830-7843.
4. Kale, L., R. Skeel, M. Bhandarkar, R. Brunner, A. Gursoy, N. Krawetz, J. Phillips, A. Shinozaki, K. Varadarajan, and K. Schulten. 1999. NAMD2: Greater scalability for parallel molecular dynamics. J Comp Phys 151:283-312.
5. Feller, S. E., Y. H. Zhang, R. W. Pastor, and B. R. Brooks. 1995. Constant pressure molecular dynamics simulation: the Langevin piston method. J Chem Phys 103:4613-4621.
6. Essmann, U., L. Perera, M. L. Berkowitz, T. Darden, H. Lee, and L. G. Pedersen. 1995. A smooth particle mesh Ewald method. J Chem Phys 103:8577-8593.
7. Izaguirre, J. A., S. Reich, and R. D. Skeel. 1999. Longer time steps for molecular dynamics. J Chem Phys 110:9853-9864.

8. Andersen, H. C. 1983. Rattle: a "velocity" version of the shake algorithm for molecular dynamics calculations. J Comput Phys 52:24-34.
9. Venable, R. M., Y. Luo, K. Gawrisch, B. Roux, and R. W. Pastor. 2013. Simulations of anionic lipid membranes: Development of interaction-specific ion parameters and validation using NMR data. J of Phys Chem B 117:10183-10192.
10. Brooks, B. R., C. L. Brooks, 3rd, A. D. Mackerell, Jr., L. Nilsson, R. J. Petrella, B. Roux, Y. Won, G. Archontis, C. Bartels, S. Boresch, A. Caflisch, L. Caves, Q. Cui, A. R. Dinner, M. Feig, S. Fischer, J. Gao, M. Hodoscek, W. Im, K. Kuczera, T. Lazaridis, J. Ma, V. Ovchinnikov, E. Paci, R. W. Pastor, C. B. Post, J. Z. Pu, M. Schaefer, B. Tidor, R. M. Venable, H. L. Woodcock, X. Wu, W. Yang, D. M. York, and M. Karplus. 2009. CHARMM: the biomolecular simulation program. J Comput Chem 30:1545-1614.
11. Humphrey, W., A. Dalke, and K. Schulten. 1996. VMD: Visual molecular dynamics. J Molec Graphics 14:33-38.
12. MacKerell, A. D., D. Bashford, M. Bellott, R. L. Dunbrack, J. D. Evanseck, M. J. Field, S. Fischer, J. Gao, H. Guo, S. Ha, D. Joseph-McCarthy, L. Kuchnir, K. Kuczera, F. T. K. Lau, C. Mattos, S. Michnick, T. Ngo, D. T. Nguyen, B. Prodhom, W. E. Reiher, B. Roux, M. Schlenkrich, J. C. Smith, R. Stote, J. Straub, M. Watanabe, J. Wiorkiewicz-Kuczera, D. Yin, and M. Karplus. 1998. All-atom empirical potential for molecular modeling and dynamics studies of proteins. J Phys Chem B 102:3586-3616.
13. Grauffel, C., B. Yang, T. He, M. F. Roberts, A. Gershenson, and N. Reuter. 2013. Cation−π interactions as lipid-specific anchors for phosphatidylinositol-specific phospholipase C. J Am Chem Soc 135:5740-5750.
14. Minoux, H., and C. Chipot. 1999. Cation-π interactions in proteins: Can simple models provide an accurate description? J Am Chem Soc 121:10366-10372.
15. Giorgino, T. 2014. Computing 1-D atomic densities in macromolecular simulations: The density profile tool for VMD. Comput Phys Commun 185:317-322.
16. Baker, N. A., D. Sept, S. Joseph, M. J. Holst, and J. A. McCammon. 2001. Electrostatics of nanosystems: Application to microtubules and the ribosome. Proc Natl Acad Sci USA 98:10037-10041.
17. Mackerell, A. D., M. Feig, and C. L. Brooks. 2004. Extending the treatment of backbone energetics in protein force fields: Limitations of gas-phase quantum mechanics in reproducing protein conformational distributions in molecular dynamics simulations. J Comput Chem 25:1400-1415.
18. Gilson, M. K., and B. H. Honig. 1987. Calculation of electrostatic potentials in an enzyme active site. Nature 330:84-86.
19. Cheng, J., S. Karri, C. Grauffel, F. Wang, N. Reuter, M. F. Roberts, P. L. Wintrode, and A. Gershenson. 2013. Does changing the predicted dynamics of a phospholipase C alter activity and membrane binding? Biophys J 104:185-195.
20. Middleton, E. R., and E. Rhoades. 2010. Effects of curvature and composition on α-synuclein binding to lipid vesicles. Biophys J 99:2279-2288.
21. Rusu, L., A. Gambhir, S. McLaughlin, and J. Radler. 2004. Fluorescence correlation spectroscopy studies of peptide and protein binding to phospholipid vesicles. Biophys J 87:1044-1053.

22. Thompson, N. L. 1991. Fluorescence correlation spectroscopy. In Topics in Fluorescence Spectroscopy. J. R. Lakowicz, editor. Plenum Press, New York. 337-378.
23. Magde, D., E. L. Elson, and W. W. Webb. 1974. Fluorescence correlation spectroscopy. 2. Experimental realization. Biopolymers 13:29-61.
24. Elson, E. L., and D. Magde. 1974. Fluorescence correlation spectroscopy. 1. Conceptual basis and theory. Biopolymers 13:1-27.
25. Murray, D., A. Arbuzova, G. Hangyas-Mihalyne, A. Gambhir, N. Ben-Tal, B. Honig, and S. McLaughlin. 1999. Electrostatic properties of membranes containing acidic lipids and adsorbed basic peptides: theory and experiment. Biophys J 77:3176-3188.
26. Murray, D., A. Arbuzova, B. Honig, and S. McLaughlin. 2002. The role of electrostatic and nonpolar interactions in the association of peripheral proteins with membranes. In Current Topics in Membranes. T. J. M. Sidney A. Simon, editor. Academic Press. 277-307.
27. Mulgrew-Nesbitt, A., K. Diraviyam, J. Wang, S. Singh, P. Murray, Z. Li, L. Rogers, N. Mirkovic, and D. Murray. 2006. The role of electrostatics in protein-membrane interactions. Biochim Biophys Acta 1761:812-826.
28. Lumb, C. N., and M. S. P. Sansom. 2012. Finding a needle in a haystack: The role of electrostatics in target lipid recognition by PH domains. PLoS Comput Biol 8:e1002617.